HYPERVELOCITY LAUNCHER IMPROVEMENT TECHNIQUES

J. R. DeWitt and D. T. Akers
ARO, Inc.

December 1972

VON KÁRMÁN GAS DYNAMICS FACILITY
ARNOLD ENGINEERING DEVELOPMENT CENTER
AIR FORCE SYSTEMS COMMAND
ARNOLD AIR FORCE STATION, TENNESSEE

NOTICES

When U. S. Government drawings specifications, or other data are used for any purpose other than a definitely related Government procurement operation, the Government thereby incurs no responsibility nor any obligation whatsoever, and the fact that the Government may have formulated, furnished, or in any way supplied the said drawings, specifications, or other data, is not to be regarded by implication or otherwise, or in any manner licensing the holder or any other person or corporation, or conveying any rights or permission to manufacture, use, or sell any patented invention that may in any way be related thereto.

Qualified users may obtain copies of this report from the Defense Documentation Center.

References to named commercial products in this report are not to be considered in any sense as an endorsement of the product by the United States Air Force or the Government.

HYPERVELOCITY LAUNCHER IMPROVEMENT TECHNIQUES

J. R. DeWitt and D. T. Akers
ARO, Inc.

FOREWORD

The research reported herein was conducted by the Arnold Engineering Development Center (AEDC), Air Force Systems Command (AFSC), under Program Element 65802F.

The results presented were obtained by ARO, Inc. (a subsidiary of Sverdrup & Parcel and Associates, Inc.), contract operator of AEDC, Arnold Air Force Station, Tennessee, under Contract F40600-73-C-0004. The results of the research were obtained between July 1970 and June 1972 under ARO Project Nos. VG5118 and VG5218. The manuscript was submitted for publication on July 24, 1972.

This technical report has been reviewed and is approved.

ULES L. BARNWELL
Major, USAF
Directorate of Technology

ROBERT O. DIETZ
Acting Director
Directorate of Technology

ABSTRACT

The purpose of this work was to reduce the damage to models caused by the launching accelerations in a hypervelocity launcher. A diaphragm test device was modified to better simulate conditions at diaphragm release in a hypervelocity launcher. Modification allowed hydrogen to be used as the test gas and a sabot to be placed in a short launch tube downstream of the diaphragm. Pressure transducers on both sides of the diaphragm were used to monitor the opening characteristics of various diaphragms. It was determined that diaphragms with tapered web thicknesses could be designed to produce pressure-time histories on the base of sabots that were less conducive to production of damaging transient stress waves in the sabots. The dynamic stress waves in a model and sabot and their interactions were measured experimentally in the diaphragm test device for a 10-deg semiangle cone model and sabot package typical of those launched in the AEDC 1000-ft Range G. Only the initial part of the motion in the launcher was duplicated using standard G-Range diaphragm, model, and sabot. The stresses were measured by strain gages cemented to portions of the model and sabot. Although there was considerable scatter in the data, the measurements indicated that the initial stress wave, in most cases, amplified on passing from the sabot into the base of the model. The stress wave further amplified under some conditions as it traveled into the nose of the model, indicating the probable cause of nose tip failure which has occurred in actual launches. Recommendations are included for further testing to better understand the stress waves and their interactions during launch of a model-sabot package by a hypervelocity launcher.

CONTENTS

APPENDIXES

I. ILLUSTRATIONS

Figure

II. TABLES

NOMENCLATURE

A	Identification for pressure data curve
B	Identification for sabot data curve
C	Identification for model location 1, longitudinal gage data curve
D	Identification for model location 1, hoop gage data curve
E	Tensile modulus of elasticity, psi
F	Identification for model location 2, longitudinal gage data curve
σ	Compressive stress, psi
ϵ	Strain, μ in./in.
ϵ'	Strain/displacement, μ in./in.
μ	Poisson's ratio

SUBSCRIPTS

r	Radial direction
z	Longitudinal direction
θ	Tangential direction
1	Model location 1
2	Model location 2
3	Model location 3

SECTION I
INTRODUCTION

Efforts in the past to optimize the launch cycles of the hypervelocity launchers used in the VKF hyperballistic ranges (Refs. 1, 2, and 3) have concentrated primarily on reducing the maximum acceleration to which the model-sabot package has been subjected in the launch tube. These efforts were directed toward producing a more uniform or "constant" base pressure launch cycle. Included in the work were improvements to the launch cycle computer program used to predict theoretical launcher kinematics (Ref. 1), such as accounting for real gas effects, approximation of losses because of viscous gas, heat transfer to the walls of the launcher, piston friction, and plastic deformation (Ref. 3). Launcher charge conditions were then predicted which would produce more optimum launch cycles. These predictions were compared with experimental data which included launch velocity, kinematics of the projectile as measured by a microwave reflectometer (Ref. 4), and measurement of pressure-time histories at various points in the launcher.

The advent of ablation material testing and the need for ablation resistant nose tips on models used for aerodynamic testing at high Reynolds numbers has added another criterion to the constraints needed to produce an optimum cycle. This was the control of transient stresses produced in the model-sabot package at the start of projectile motion (diaphragm opening) and at release of the base pressure at exit from the launch tube.

Ablation resistant materials such as graphite are typified by a brittle failure mode and low strength. Thus, it is possible to produce transient stresses in the model of such a magnitude as to cause tensile failure in the nose tip material.

This report considers two approaches used to better understand the problem and to reduce the magnitude of the transient stresses. The first is concerned with reducing the transient pressure loads at diaphragm opening and at muzzle exit and the second with the strain gaging of a model-sabot package to determine the transient stresses in the package.

SECTION II
DIAPHRAGM TEST DEVICE

An existing diaphragm test device (Fig. 1a, Appendix I) was modified (Fig. 1b) to better simulate the actual launcher conditions at the time of diaphragm opening. The original device used gun powder for gas generation. When the diaphragm burst, the small reservoir of gas was quickly vented to atmosphere. Thus only diaphragm burst pressure could be determined by the pressure transducer output.

The modified test device consisted of a reservoir of hydrogen which was compressed by gun powder combustion to rupture the diaphragm. A slug representing a typical model-sabot package weight was placed in the stub barrel for the diaphragm development tests to simulate flow conditions downstream of the diaphragm. Pressures on both sides of the diaphragm were measured to determine the diaphragm opening characteristics, so that meaningful changes in diaphragm design could be identified. Figure 2 gives a typical pressure-time history upstream of the diaphragm for a 5000-psi burst pressure.

The stub barrel also allowed a strain-gage instrumented model-sabot package to be tested to determine transient stresses at the time of diaphragm opening. Standard diaphragms as used in the VKF G04 launcher (2.5-in.-diam launch tube bore) were used in these tests with the strain-gaged models.

SECTION III
MODIFIED DIAPHRAGMS

The "constant" base pressure launch from a hypervelocity launcher requires that the diaphragm release pressure, the maximum base pressure, and the muzzle exit pressure must be equal. Past experience with the VKF launchers has demonstrated that operation at release pressures well below that required for constant base pressure conditions was necessary for survival of fragile nose tips.

This indicated that the combination of the time rate of increase of the base pressure at release and its magnitude produced the transient stress waves which broke the nose tips. The magnitude of the base pressure produced at diaphragm release is, of itself, not sufficient to break nose tips since the maximum base pressure generated later in the launch cycles now in use exceeds the "constant" base pressure value.

Figure 3 gives the pressure-time history at the diaphragm of the G04 launcher as extrapolated from pressure measurements made near the diaphragm for a typical ablation model shot. The diaphragm release point is indicated for the standard 3200-psi release pressure diaphragms used on these shots. The driver gas compression process is seen to be a series of shock waves causing sharp pressure rises with the gradual increase caused by compression waves between these shocks.

One method of reducing the time rate of pressure application on the base of the sabot would be to use a diaphragm which opens partially on one of these shock waves and opens more fully with the increasing pressure. Thus, at the intermediate stages of opening, the diaphragm would act as an orifice between the driver gas and the sabot. This orifice effect would slow the sabot motion and would have an effect on the launch cycle similar to a higher release pressure diaphragm. The approach used to accomplish this was to increase the remaining metal thickness (web thickness, Fig. 4) at the base of the grooves with distance from the center of the diaphragm. This was done by two methods. The first was to taper the diaphragm on the side opposite the grooves which produced a variation of total petal thickness as well as the web thickness. The second method was to taper the groove depth from the center of the diaphragm. This left a constant petal thickness.

Figure 4 shows the standard diaphragm design which has a nominal burst pressure of 3200 psi. The petal thickness and the groove depth are constant. The material for this design and for all the modified diaphragms was hot rolled type 304 stainless steel. Figures 5 and 6 give pressure-time histories between the diaphragm and sabot for two of the standard diaphragms. These diaphragms produce a pressure rise time of approximately 150 to 200 μsec. These two figures show that some variation in opening characteristics must be expected with a given design. All burst pressures quoted in this report are nominal with a variation of approximately ±5 percent to be expected. It should be noted that the maximum pressure measured between the diaphragm and sabot does not necessarily correlate with the burst pressure.

Figure 7 gives the design details and burst pressures of the first seven types of modified diaphragms tested. These all were tapered on the side opposite the grooves. Figure 8 gives the pressure-time history between the diaphragm and sabot for the type 3 diaphragm (8-deg taper). Rise time for the pressure pulse was greater than 1.5 msec even with twice the burst pressure as compared with the 150 to 200 μsec for the standard diaphragm. The types 1 and 2 showed similar pressure time histories. Figure 9 gives the pressure time history between the diaphragm and sabot for the type 4 (5-deg taper) diaphragm.

Total rise time is over 1 msec, but the trace shows some tendency toward a rapid opening. Fig. 10 gives the pressure-time history between the diaphragm and sabot for the type 6 (4-deg taper) diaphragm which gave as rapid a pressure rise time as the standard diaphragm. This was also true for the type 7 (3-deg taper) diaphragm as may be seen from Fig. 11.

Figure 12 gives the design details of the type 8 (3- to 9-deg taper) diaphragm which had a nominal burst pressure of 5000 psi. Figure 13 gives the pressure-time history between the diaphragm and sabot for this type diaphragm. Some improvement in opening characteristics may be seen as compared with the standard and type 6 and 7 diaphragms.

The next iterations in design are given by Fig. 14 along with the burst pressures. Types 9 and 10 have tapered grooves and constant petal thickness. Figure 15 gives the pressure-time history between the diaphragm and sabot for the type 9 (5-deg tapered groove) diaphragm which had a rise time of approximately 600 μsec. Figure 16 gives the pressure-time history between the diaphragm and sabot for the type 10 diaphragm which showed no improvement in opening characteristics over the standard diaphragm.

The type 9 diaphragm was selected for further tests in the G04 launcher. With the burst pressure increase from 3200 to 4900 psi, it was possible to increase the piston weight from the normal 110 to 130 lb without incurring excessive piston impact on the diaphragm holder in the high-pressure section. Other charge conditions were 115-psia hydrogen in the pump tube and a 317-gram polycarbonate slug. Figure 17 gives a comparison between acceleration reduced from the microwave reflectometer data (Ref. 4) and that from the computed cycle. The microwave data ended after 20 ft of projectile travel because reflection from the plasma formed in the air in the launch tube ahead of the projectile. The computation was based on a 5000-psi release pressure. Reasonable agreement is seen between the experimental and theoretical results as the experimental launch velocity was 19,200 ft/sec and the computed velocity was 18,900 ft/sec.

It is interesting to compare this cycle computation with the computation for the standard 18,000-ft/sec shot conditions used for ablation material tests. Figure 18 gives the comparison between these two conditions. Computed velocity for the ablation test condition was 18,600 ft/sec with a 290-gram model-sabot package weight. The modified diaphragm cycle shows a reduction in peak acceleration of approximately 25 percent even with a slightly higher launch velocity. Whether the modified diaphragm maintains its measured opening characteristics

in the launcher is yet to be determined and will be inferred primarily by its effect on a fragile nose model.

SECTION IV
LAUNCH TUBE EXTENSION

In an effort to reduce transient stresses in the model at muzzle exit, the G04 launch tube was extended from 42 to 54 ft. Calculations using the launcher computation theory (Ref. 3) indicated that the maximum acceleration to which the model-sabot package would be subjected would be reduced by approximately 14 percent for the 18,000-ft/sec launch velocity regime of the typical ablation model tests. Also muzzle exit pressure would be reduced approximately 43 percent, which should reduce the stress waves in the model produced by the unloading of the model at the muzzle exit. The extended launch tube has performed as expected and has increased survivability of the ablation models. The calculations made for the extended launch tube case are compared in Figs. 17 and 18 with experimental results.

SECTION V
DESCRIPTION OF TEST SETUP FOR MEASUREMENT OF DYNAMIC STRESS INTERACTIONS IN MODELS AND SABOTS

The model configuration used for this study, a 10-deg semiangle cone, was chosen to simulate the configuration used by Evans (Ref. 5). The models (Fig. 19) were made of 7075-T6 aluminum with a tensile modulus of elasticity of $10.4\ (10)^6$ psi, a tensile ultimate strength of 83,000 psi, and a tensile yield strength of 73,000 psi.

The sabots (Fig. 20) were made of Lexan® with a tensile modulus of elasticity of 345,000 psi, a tensile ultimate strength of 9,500 psi, and a tensile yield of 9,000 psi.

All strain data were measured using foil electric resistance strain gages. The gages were located as shown on Figs. 19 and 20. The gage on the sabot had a gage length of 0.125 in., a resistance of 120.0 ohms, and a gage factor of 2.01. The gages used on the model were 0.031 in. long, had a resistance of 120.0 ohms, and a gage factor of 1.95. The gages were bonded to the sabot and model using an epoxy cement cured at room temperature.

Figure 21 shows a model-sabot package assembly ready to be loaded into the diaphragm test device (Fig. 1). The strain-gage leads extending out in front of the sabot are carefully loaded ahead of the package and pulled through the barrel before it is assembled to the high-pressure section. Then the standard 1000-ft G Range diaphragm (Fig. 4) is loaded followed by the diaphragm petal guide which is lined up to match the pressure transducer port (Fig. 1), between the diaphragm and the sabot, so as to obtain pressure readings near the model base at the instant of diaphragm rupture. The strain-gage leads are soldered to a connector in a numbered sequence to correspond to the gage locations. Then leads from the appropriate gage circuit, in the portable circuit board constructed for this test, are attached to the external pins of the instrumentation connector. Both types of gage circuits used in these tests are shown in Figs. 22 and 23. The bridge type circuit has been used many times before for work where the signal generated by bending strain needed to be eliminated. Calibration and zeroing of the bridge circuit followed the procedure outlined in Ref. 5. The potentiometer circuit has also been used commonly for dynamic strain measurements. Calibration procedure for this circuit can be found in Appendix III. During strain-gage calibration, the pressure transducers (Fig. 1) were calibrated and calibration printouts were recorded for each shot (or set of shots). The circuit board was powered by a regulated DC supply and transmitted the strain gage data through a DC amplifier to another circuit board that is permanently connected to the magnetic tape recorder in the VKF 1000-ft G Range control room. After recording, the tape was played back at a reduced speed through an oscillograph which wrote the strain data with a time base.

SECTION VI
DISCUSSION OF INDIVIDUAL TESTS FOR MEASUREMENT OF DYNAMIC STRESS INTERACTIONS IN MODELS AND SABOTS

Five tests generated enough data to warrant discussion.

Test number 1 (Fig. 24) was made primarily to check wave amplification in the nose tip (i.e., the increase in stress as the wave travels along the body). Strains were to be measured as close as 0.5 in. from the nose tip. The strain gage rosette at this location indicated reasonable data at one of the 120-deg gages, but one gage displayed high strains, and the oscillograph playback showed this circuit to have had noise or strain reading before the diaphragm ruptured, making the data very questionable. However, the longitudinal strain measuring gage (gage mounted along model centerline) in the rosette recorded data of the ex-

pected magnitude and displayed "ringing" (alternating compression and tension) of the nose. This "ringing" was not expected because the reflection of the stress wave was almost instantaneous at this location, and the input pressure pulse duration was long compared with the measurement time of the data. The combination of pressure pulse and reflections would cause the so called "ringing." The other gage, 120-deg off longitudinal, indicated almost no strain, which can be interpreted in one of two ways: either the gage was not indicating properly or there was no strain to be measured. Although the strain should be low at this location and orientation, the strain from the longitudinal component alone should be greater than was indicated. The longitudinal measuring strain gage at location 1 (rear) (Fig. 19) showed a typical strain measurement. The hoop (tangential) gage, however, indicated a very high tangential strain. There was nothing unexpected about the shape of the wave except for its sign. One would have expected the hoop stress to be tensile if it were due to the Poisson effect caused by the compressive pulse traveling down the model. However, the gage indicated a compressive hoop stress. Possibly the squeezing effect applied to the model by the sabot during launch could cause some compressive hoop stress, but surely not of the magnitude indicated by the data.

For test number 2 (Fig. 25), measurements were made at the standard strain-gage locations 1 (rear) and 2 (nose) shown in Fig. 19. The sabot strain gage (Fig. 20) obviously failed because no signal was recorded in the oscillograph data (Fig. 25). A bridge circuit (Fig. 22) was used at location 1 (Fig. 19) to measure only the pure axial load with no bending. Presumably, the sabot should eliminate most model bending. It is suspected that one of the gages failed because the data initially indicated a compressive wave (as expected) and this abruptly changed to a tensile wave. The maximum compression value, which was very small, was used in all figures when representing test number 2 at location 1 (longitudinal strain only) although this must be considered subject to error. The signal from the hoop gage at location 1 was very similar in magnitude and form to that of test number 1 except that the strain indicated was a tensile strain while the longitudinal gage indicate compression strain, just the reverse of test number 1. The longitudinal gage at location 2 showed the ringing effect, but otherwise seems typical.

Test number 3 (Fig. 26) was successful in that all strain gages seemed to be functioning properly with the one exception of sign convention. Initially all strain-gage channels were to be connected such that a downward deflection on the oscillograph playback indicated a compressive strain. However, for this particular test, the instrumentation was to be connected such that the hoop gage trace deflected upward for a compressive strain and longitudinal gages trace deflected downward for a

compressive strain. Thus, the data shown in Fig. 26 seem to indicate a tensile wave in the longitudinal direction and a compressive wave in the hoop direction. Unfortunately, posttest instrumentation checks were impossible since the model, sabot, and instrumentation cable were destroyed. It will be assumed that there was an instrumentation error somewhere, and the longitudinal gage data are plotted as compressive in all representations of test number 3.

After observing the discrepancies in the sign (indicating tension or compression) of the strain data on previous tests, special care was taken in pretest instrumentation checkout for tests number 4 and 5 (Figs. 27 and 28). The instrumentation setup was such that model longitudinal gage data would deflect upward for compressive strain and hoop gage data would deflect downward for compressive strain. With the above sign conventions well in mind, a discussion of tests number 4 and 5 follows.

Test number 4 (Fig. 27) showed a tensile strain initially at location 1 (Fig. 19), in spite of the fact that a compressive load was applied. The sabot data also have an oddity in that they started as a compressive wave but rapidly became a large tensile strain wave. The hoop gage also indicated a compressive wave initially and then reversed almost in phase with the aforementioned sabot gage reading. The longitudinal strain gage at location 2 (Fig. 19) was the only one that displayed a compression wave and maintained this sign throughout data measurement. One possible explanation for the peculiar behavior of most of the gages was the unusual diaphragm opening. As displayed by the pressure transducer trace (Fig. 27), the maximum pressure was attained by a series of step pulses developed over a much longer time than for previous test shots.

Test number 5 (Fig. 28) had the typical diaphragm opening as shown by the pressure data. The same anomaly with the sabot gage appeared in this test as in test number 4. That is, the gage initially read a compressive pulse (as anticipated) but gradually changed to a tensile wave. Longitudinal strain-gage data at location 1 (Fig. 19) showed a compressive wave (as expected) but the magnitude of the strain seems to be very low. The hoop gage at location 1 seemed to oscillate about zero indicating small strains. The longitudinal gage at location 2 (Fig. 19) measured data very similar to that of test number 4 and indicated the expected compressive wave.

SECTION VII
DISCUSSION OF RESULTS FOR MEASUREMENT OF DYNAMIC STRESS INTERACTIONS IN MODELS AND SABOTS

The strain-gage data for individual shots was anomalous in terms of the direction of trace deflection and thus the apparent sign of the stress. Tension waves were frequently indicated when compression waves were anticipated. In many cases special care was taken in instrumentation setup to avoid sign errors. So it is doubtful that all these "sign" anomalies can be attributed to wiring errors. There may be other unknown problems or the measurements may, in fact, be correct. Further study will hopefully clarify this situation. For purposes of this preliminary data analysis, the stress measurements are treated without regard for sign.

Stresses have been calculated from the measured strains as shown in Appendix IV, and the results are shown in Figs. 29 and 30. In almost all cases the model base stress was larger than the sabot stress (Fig. 29). While this trend was expected, based on the difference in cross-sectional areas of the two components, there may have been other contributing factors such as the assembly of the base plates to the sabot, the fit between sabot and model and the fit between base plates and model.

Figure 29, plotted from Table I (Appendix II), shows average base pressure plotted against peak stress (see Fig. 24 for clarification of average). The values of Table I were determined from test data by the method given in Appendix IV. As can be seen from Fig. 29, the data are quite scattered. The most probable cause of the wide data scatter is the fit of the base plate to the model and sabot (Fig. 21). Without a perfect fit, the loading wave could be transmitted into the model through one, two, or three segments of the base plate instead of uniformly through all four. This would cause a nonuniform pulse traveling down the model, and bending stresses would be increased significantly because of wave reflections. This could be the cause of the high nose stresses in tests numbers 2, 4, and 5. One other comment that could change the conclusions based on Fig. 29 is the test number 2 demonstrated a nose stress much higher than the base stress. This was primarily due to the low measured compressive stress at the base which abruptly became tensile. Thus, amplification of stresses in the nose is not conclusively shown in these two tests (2 and 3).

Two other tests showed higher nose stresses than base stresses. However, test number 4 had the very slow opening diaphragm that

could cause unusual stress waves. As can be seen by the data from location 1, stress magnitude was very low. It is obvious from Fig. 29 that amplification of stress from location 1 to location 2 has occurred for tests number 4 and 5. If straight lines were drawn from the origin through the various sets of data points, the data for the sabot and model location 2 give a reasonably straight line fit. However, model location 1 data are so scattered a single line is not feasible.

The strain-gage locations for this particular model and the dimensions of the model itself were chosen so that the data obtained could be compared with the data of Evans (Ref. 5). As can be seen in Fig. 30, the base stress values did correlate well with those of Ref. 5 for tests number 2, 4, and 5. However, tests number 2, 4, and 5 indicated a wave amplification in the nose region contrary to Evan's conclusions. A possible conclusion that can be drawn from this comparison is that a sabot does indeed cause stress amplification in the nose region of 10-deg semiangle cone models. This amplification could contribute to failures in nose materials with low strengths.

SECTION VIII
RECOMMENDATIONS AND CONCLUSIONS CONCERNING THE MEASUREMENT OF DYNAMIC STRESS INTERACTION IN MODELS AND SABOTS

This experiment and the experimental apparatus represent a major step from the earlier work of Evans (Ref. 5) using Hopkinson Bar apparatus. This was done with the view of simulating as exactly as possible the stressing of the model and sabot in the initial stages of motion in the G04 launcher. Thus the diaphragm, model, and sabot (including base plates) were duplicates of those used in G04, except for the sabot cutouts to allow mounting of the strain gages. The large scatter and the anomalies in the data obtained indicate that too large a step was taken, and the following recommendations are made for future work:

1. Obtain data for a solid cylinder contained in a sabot with a flat base and no backup plates.
2. Repeat, including backup plates.
3. Obtain data from sabot and solid cone.
4. Repeat with backup plates.
5. Repeat tests described in this report using a hollow cone.
6. Devise a method to ensure that there is no ambiguity as to the sign of the strain; i. e., compressive or tensile.

The conclusions from the above discussed efforts are:

1. The opening characteristics of diaphragms for a hypervelocity launcher may be altered by means of a tapered web thickness. This alteration of opening characteristics can be used to produce pressure-time histories on the base of the sabot less conducive to production of transient stress waves. In this report, only linear tapers were considered. This could not, however, be assumed the optimum type of taper.
2. Reduction of muzzle exit pressure by addition of an extension to the launch tube has increased survivability of models with fragile nose tips.
3. The study of the dynamic stresses in the model and sabot tested indicates:
   a. There is amplification of the stress in transmission between sabot and model, for most conditions.
   b. Amplification of stress in the cone can occur under some conditions.
   c. Future testing should begin with much simpler, more one-dimensional model and sabot.

REFERENCES

1. DeWitt, J. R. and Cable, A. J. "A Comparison of Experimental and Theoretical Launcher Kinematics." AEDC-TR-65-203 (AD470966), October 1965.
2. Cable, A. J., DeWitt, J. R., and Prince, M. D. "Launcher Optimization Studies." AEDC-TR-65-204 (AD471849), October 1965.
3. Cable, A. J. and DeWitt, J. R. "Optimizing and Scaling of Hypervelocity Launchers and Comparison with Measured Data." AEDC-TR-67-82 (AD812849), April 1967.
4. Hendrix, R. E. "Microwave Reflectometry in Interior Ballistics." AEDC-TR-66-54 (AD482754), May 1966.
5. Evans, P. A. "An Investigation of Elastic Strain Wave Propagation in Conical Bodies." MS Thesis, University of Tennessee Space Institute, March 1969.
6. Dalley, J. W. and Riley, W. F. Experimental Stress Analysis. New York, McGraw-Hill Book Co., 1965.

APPENDIXES

I. ILLUSTRATIONS
II. TABLES
III. CALIBRATION OF STRAIN GAGES
IV. CALCULATION OF STRESS FROM STRAIN-GAGE DATA

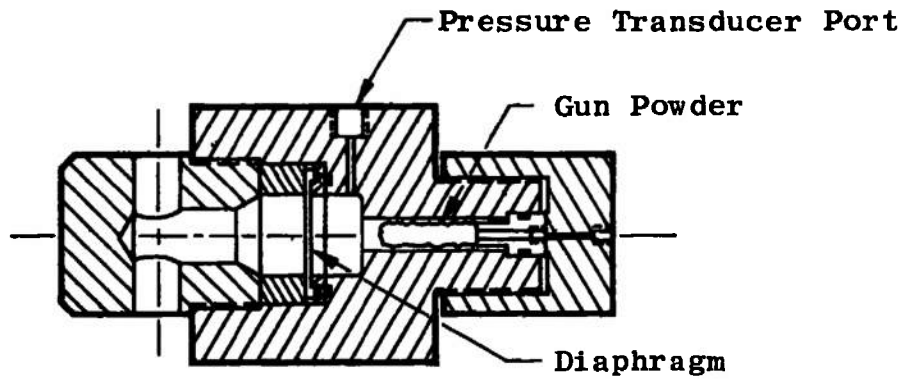

a. Original Diaphragm Test Device

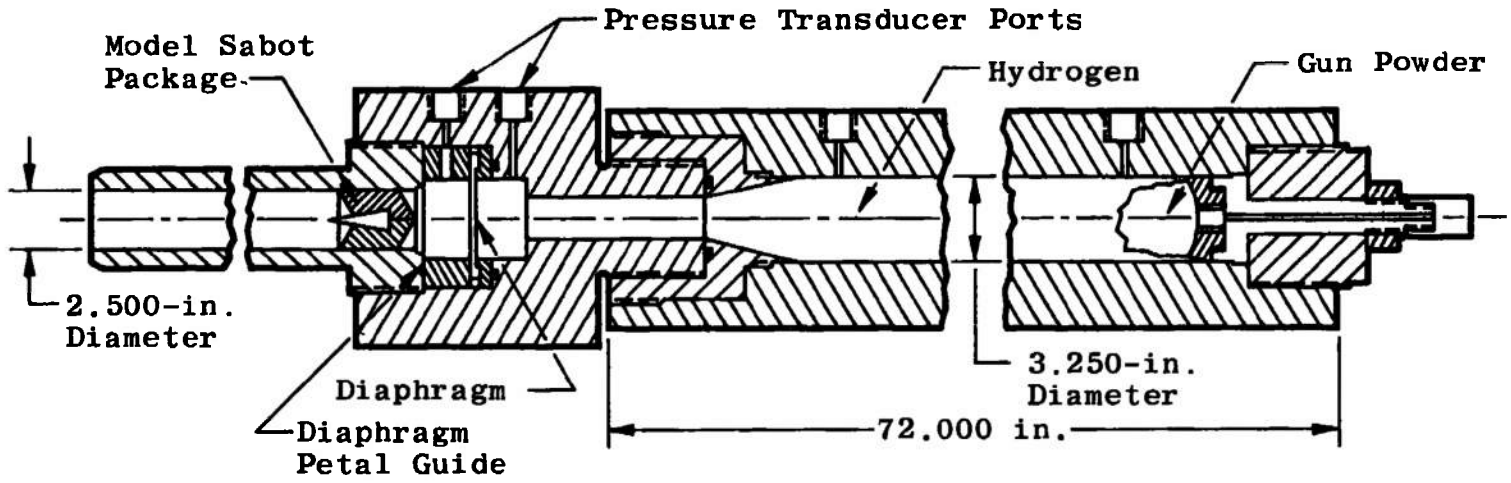

b. Modified Diaphragm Test Device

Fig. 1 Diaphragm Test Device

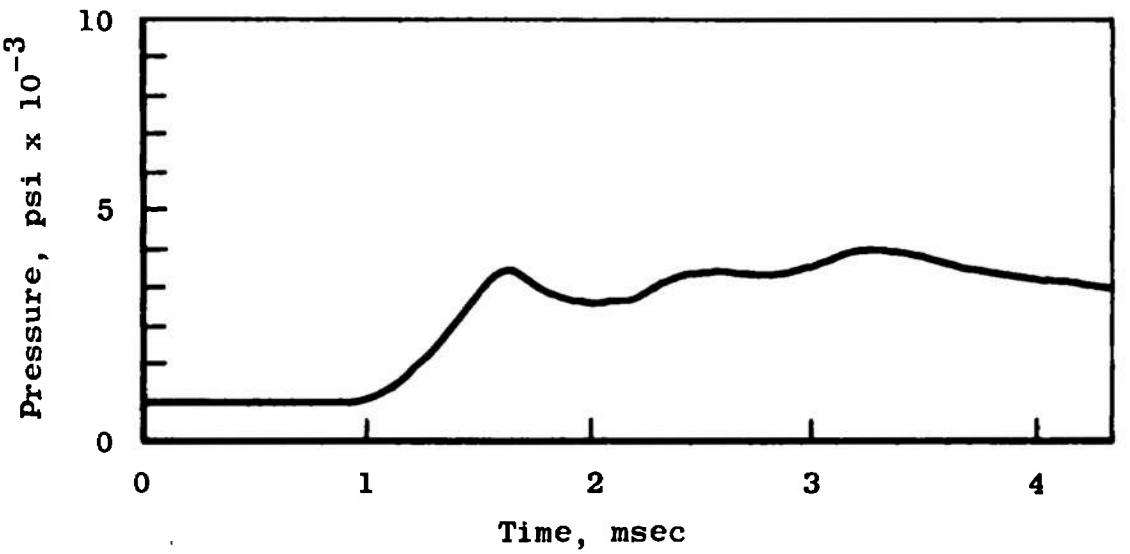

Fig. 2 Pressure-Time History Upstream of Diaphragm for 5000-psi Burst Pressure Test

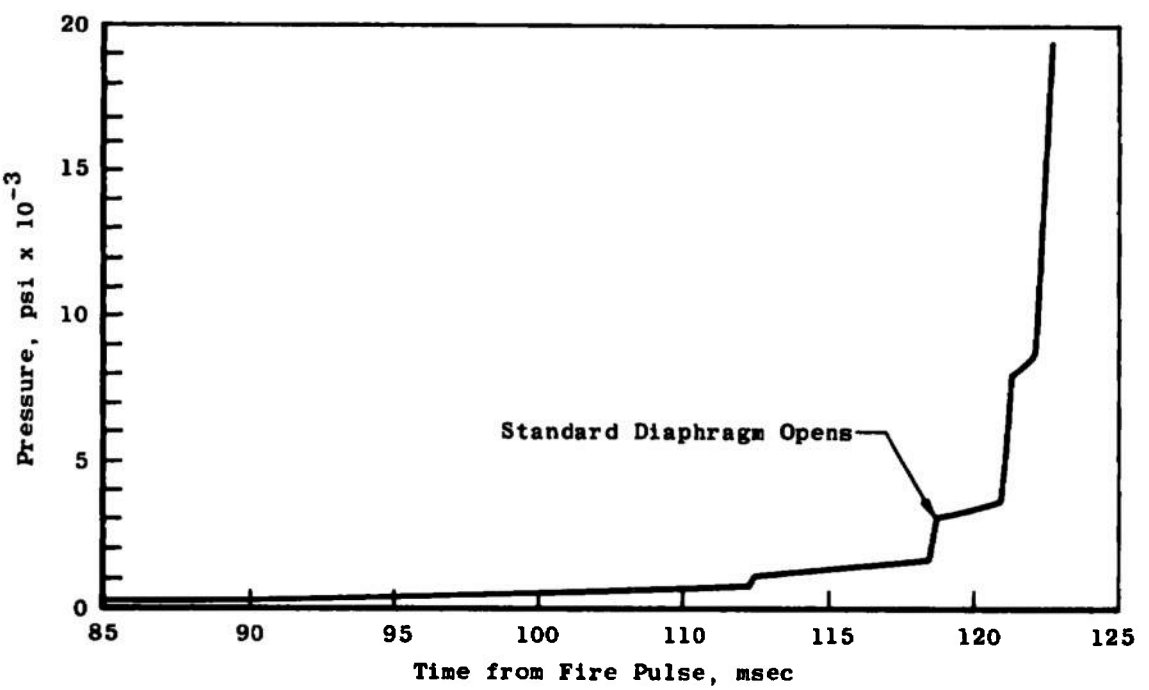

Fig. 3 Pressure-Time History at Diaphragm of G04 Launcher

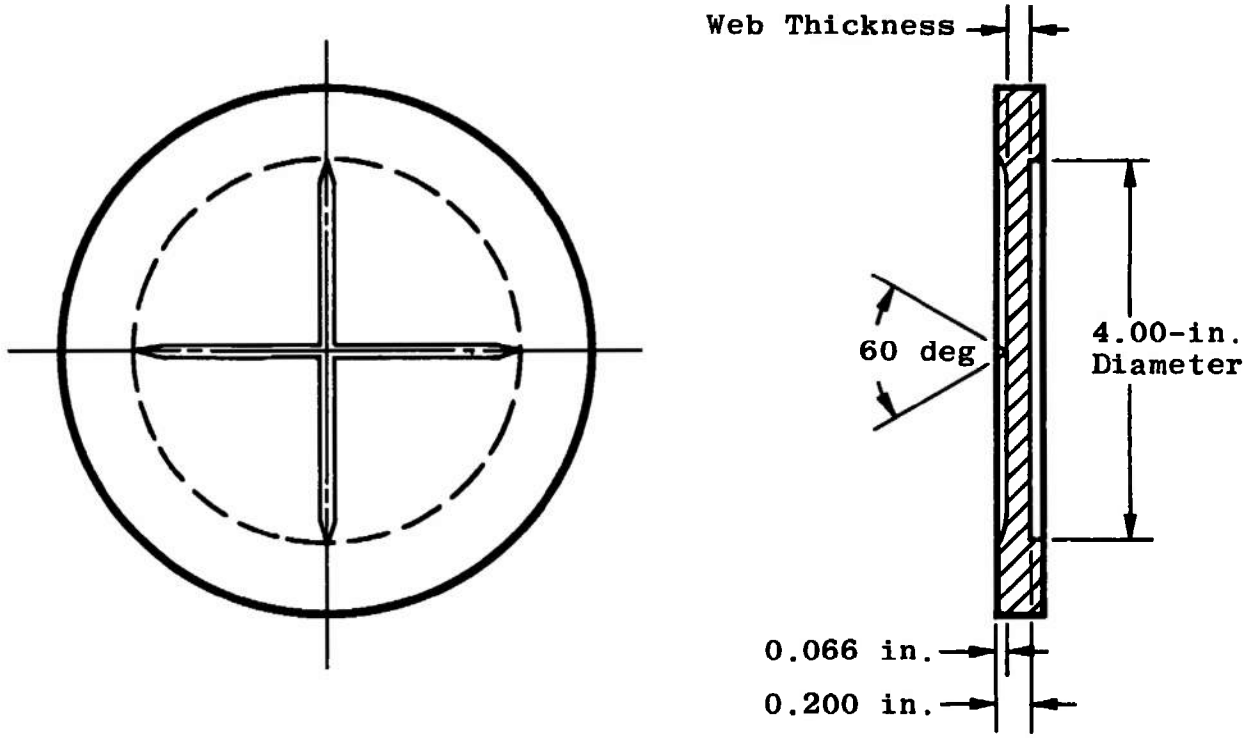

Fig. 4 Standard Diaphragm Design

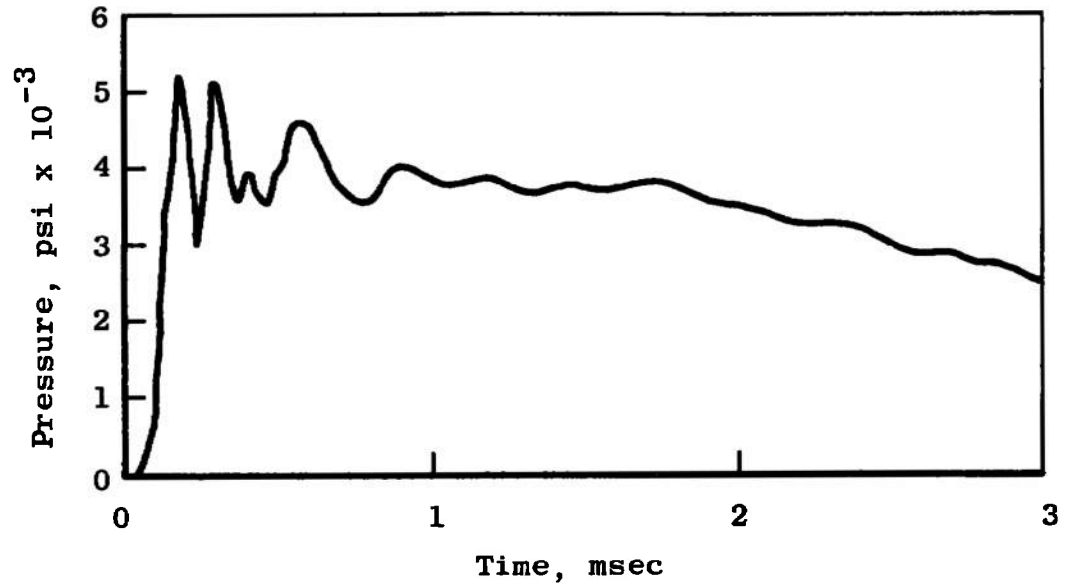

Fig. 5 Example A of Pressure-Time History for Standard Diaphragm

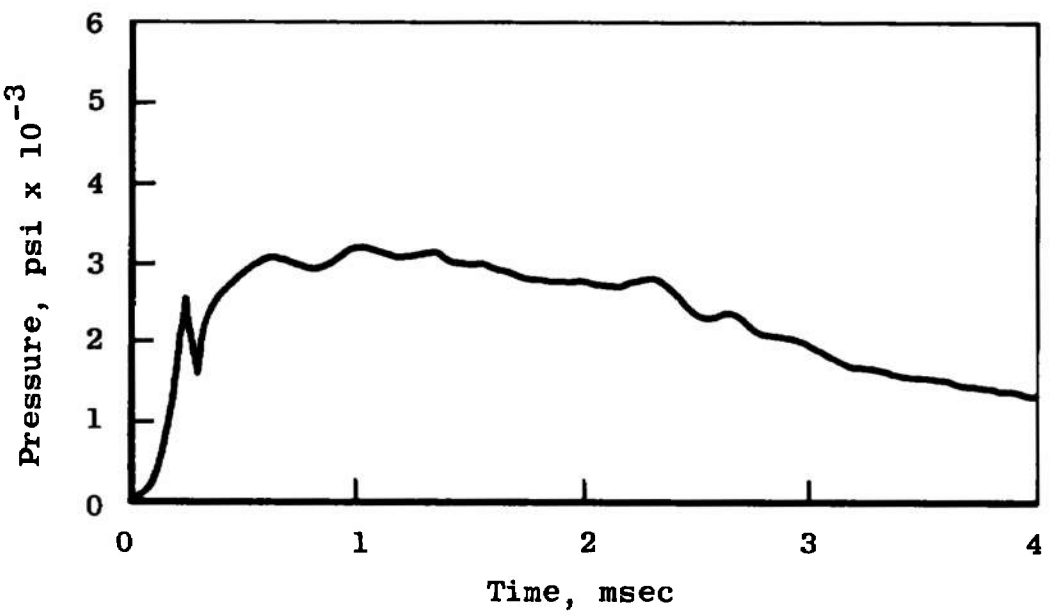

Fig. 6 Example B of Pressure-Time History for Standard Diaphragm

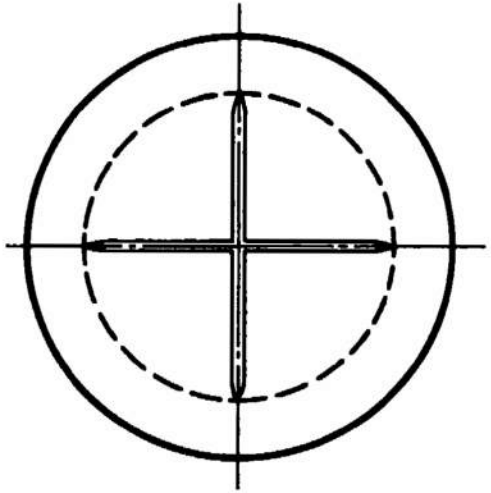

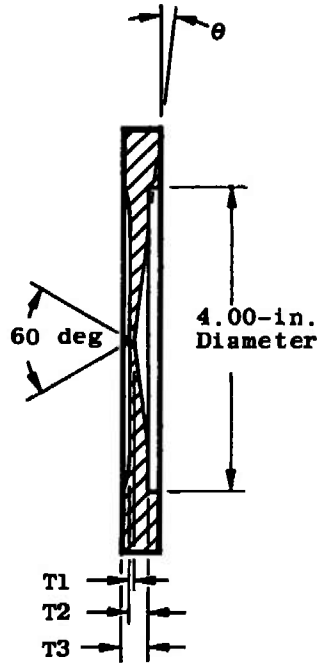

Type	θ, deg	T1, in.	T2, in.	T3, in.	Burst Pressure, psi
1	8	0.066	0.245	0.310	9000
2	8	0.038	0.245	0.310	7000
3	8	0.024	0.245	0.310	6400
4	5	0.038	0.215	0.280	5200
5	5	0.024	0.200	0.266	4800
6	4	0.024	0.164	0.230	4100
7	3	0.024	0.128	0.194	4000

Fig. 7 Modified Diaphragms—Types 1 through 7

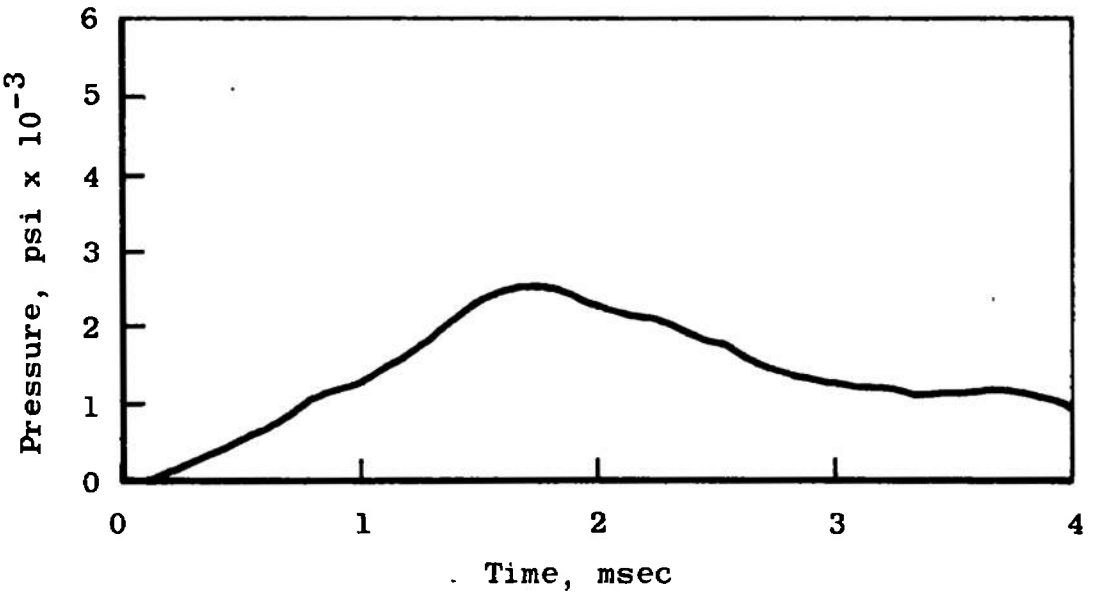

Fig. 8 Pressure-Time History for Type 3 Diaphragm

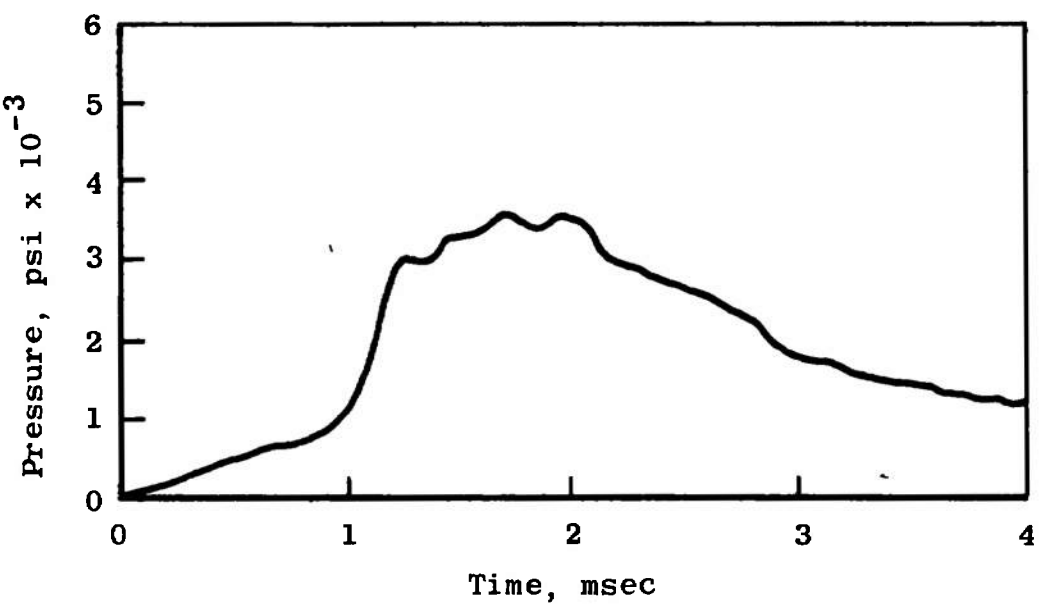

Fig. 9 Pressure-Time History for Type 4 Diaphragm

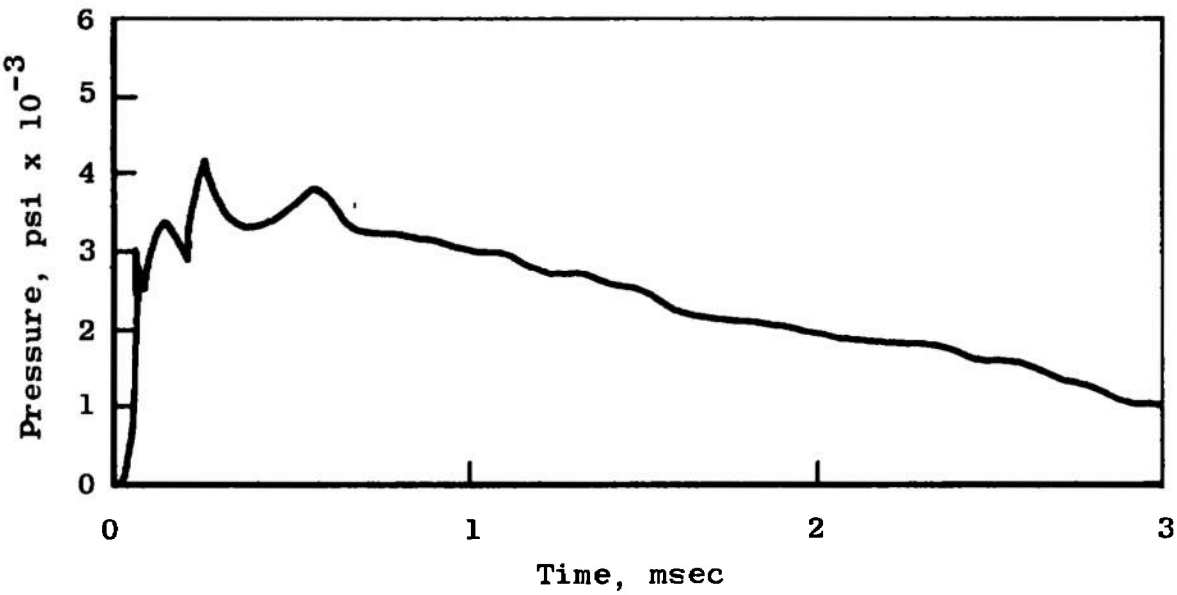

Fig. 10 Pressure-Time History for Type 6 Diaphragm

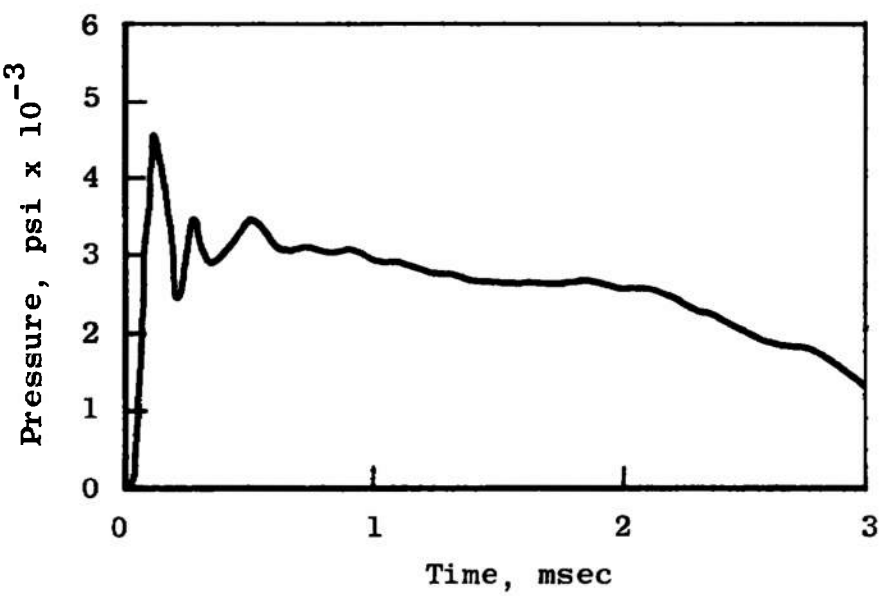

Fig. 11 Pressure-Time History for Type 7 Diaphragm

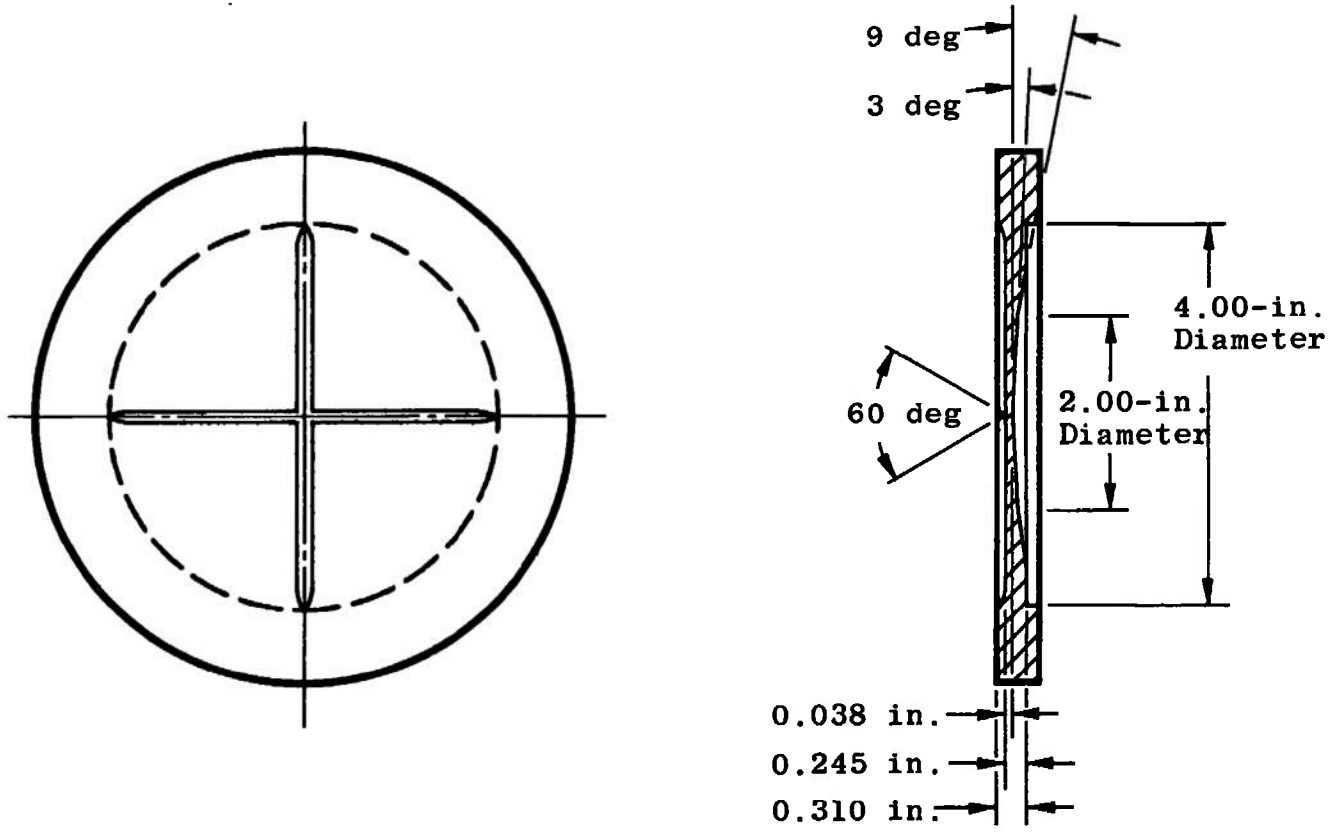

Fig. 12 Modified Diaphragm—Type 8

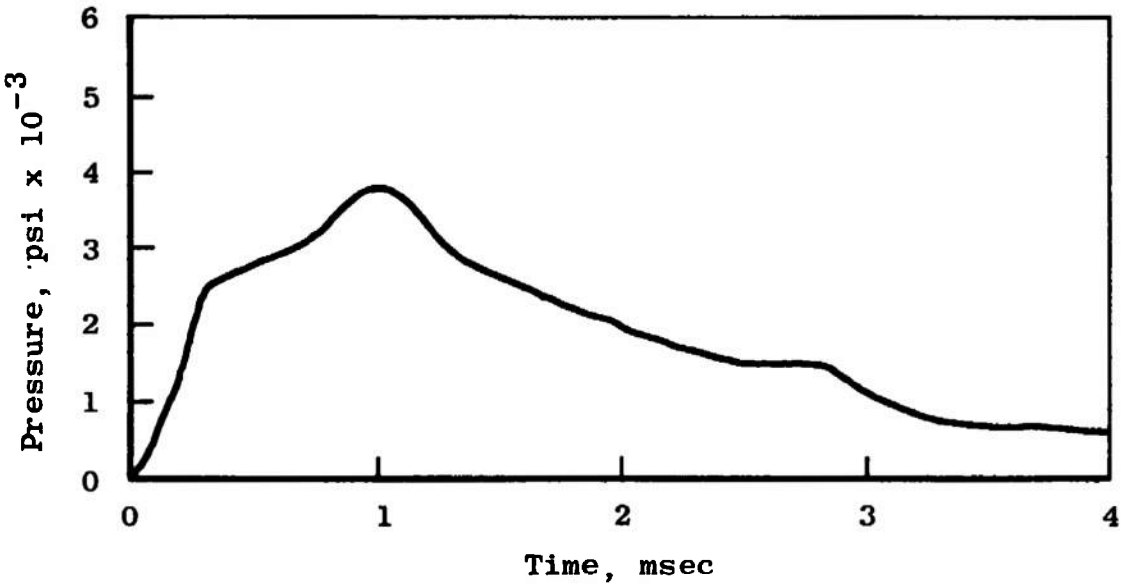

Fig. 13 Pressure-Time History for Type 8 Diaphragm

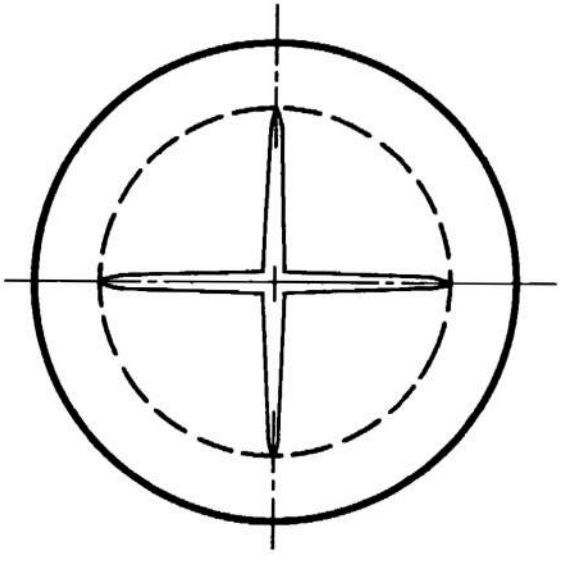

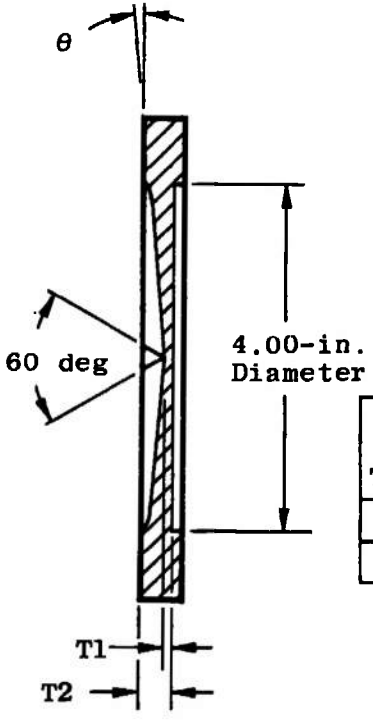

Type	θ, deg	T1, in.	T2, in.	Burst Pressure, psi
9	5	0.038	0.250	4900
10	4	0.038	0.200	4500

Fig. 14 Modified Diaphragm—Types 9 and 10

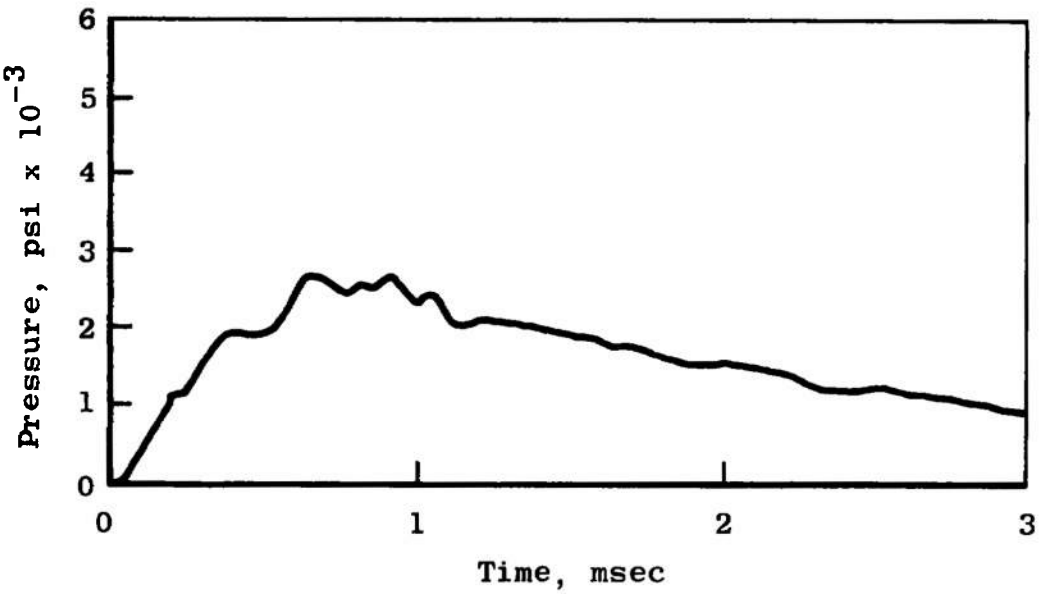

Fig. 15 Pressure-Time History for Type 9 Diaphragm

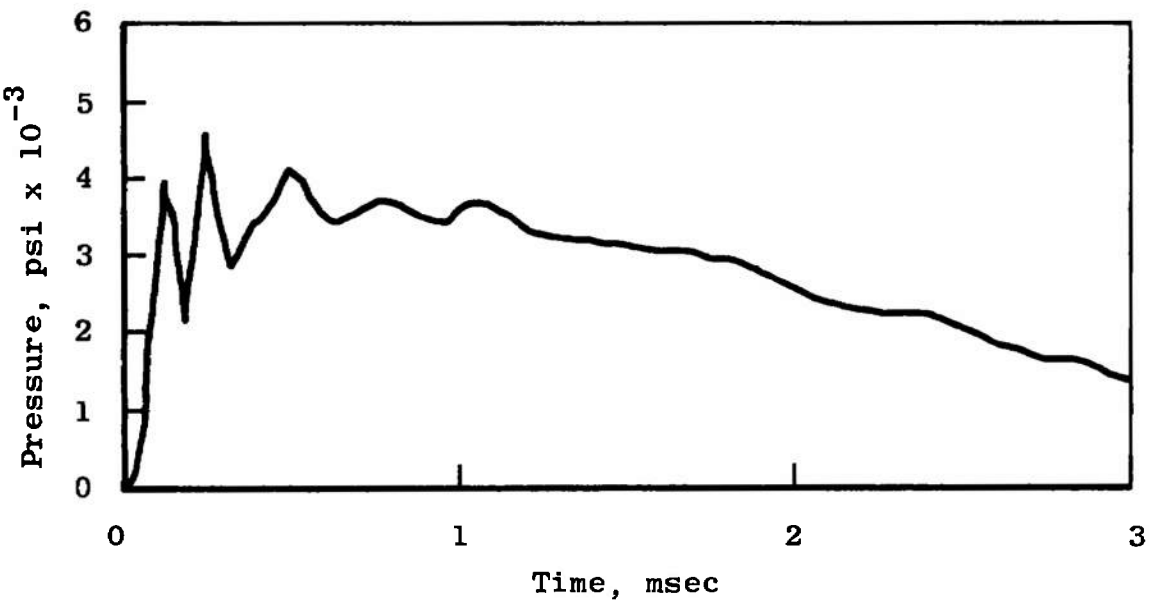

Fig. 16 Pressure-Time History for Type 10 Diaphragm

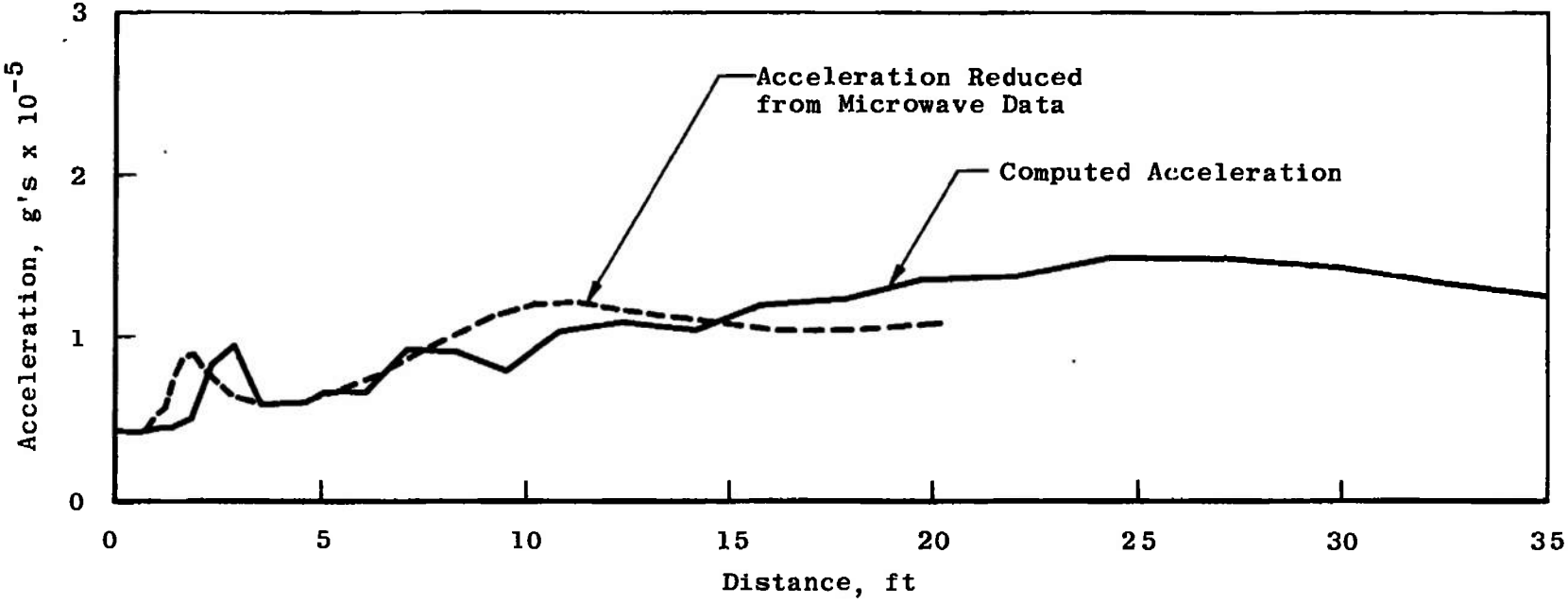

Fig. 17 Comparison of Microwave Data and Computed Acceleration for the Modified Diaphragm Shot

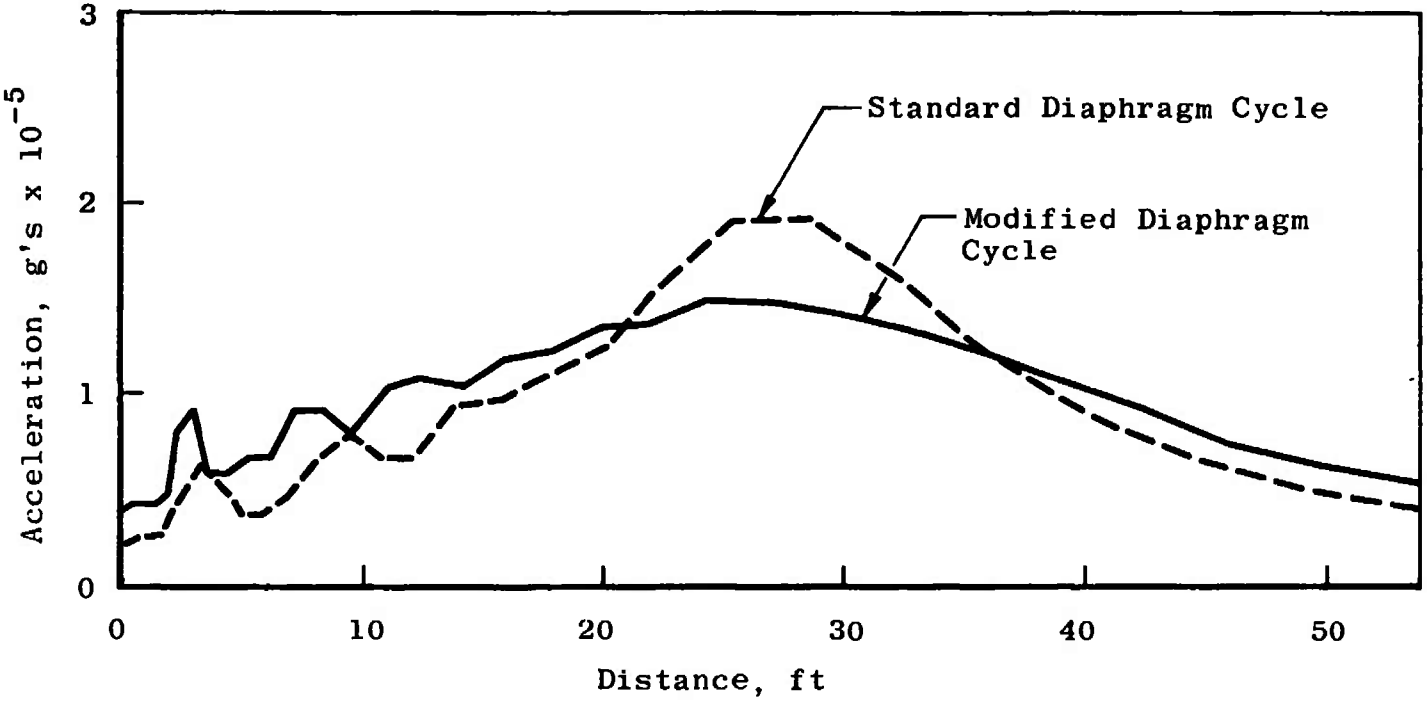

Fig. 18 Comparison of Computed Cycles for Standard Diaphragm and Modified Diaphragm

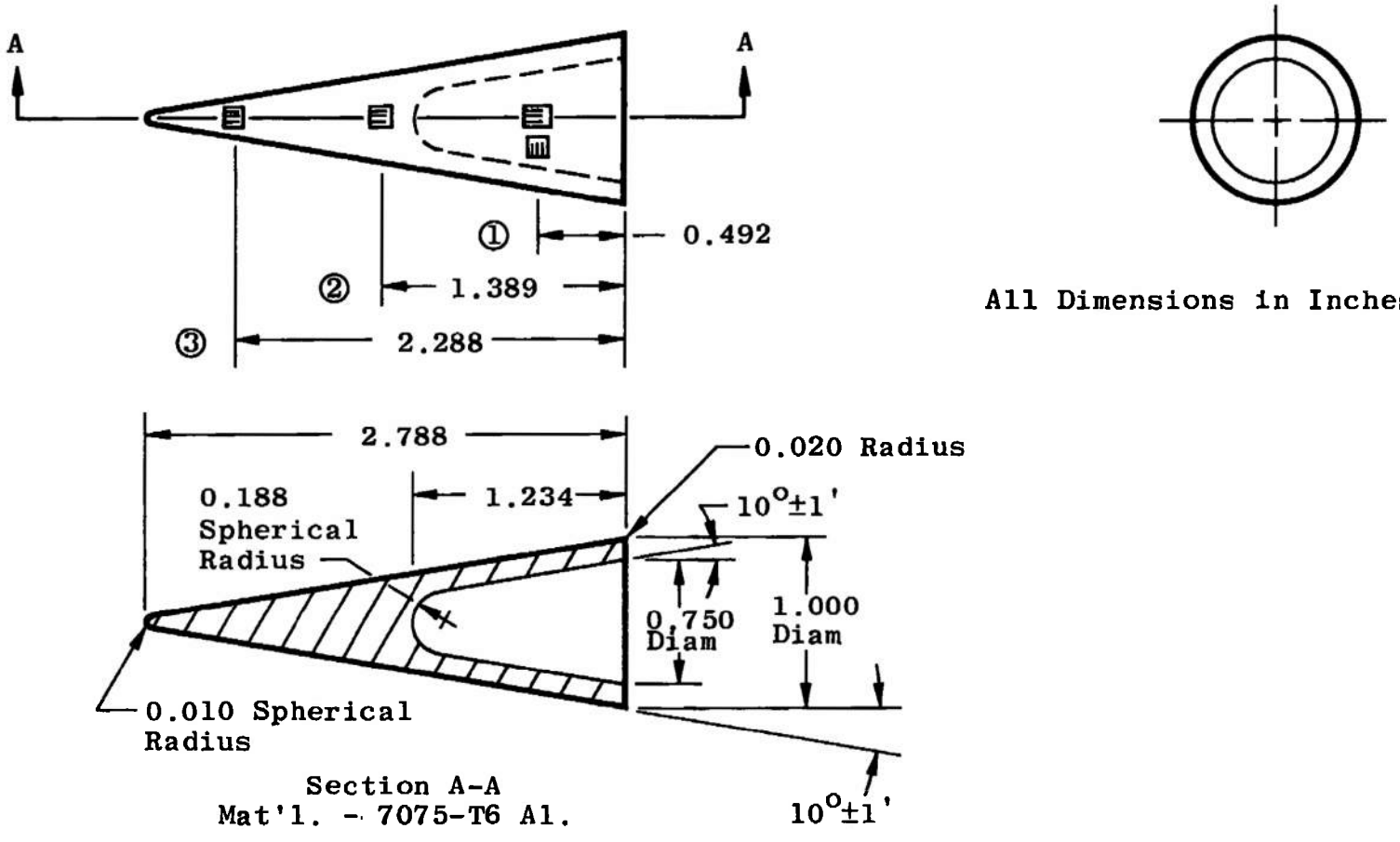

Fig. 19 10-deg Semiangle, 1.000-in. Base Diameter Cone Model

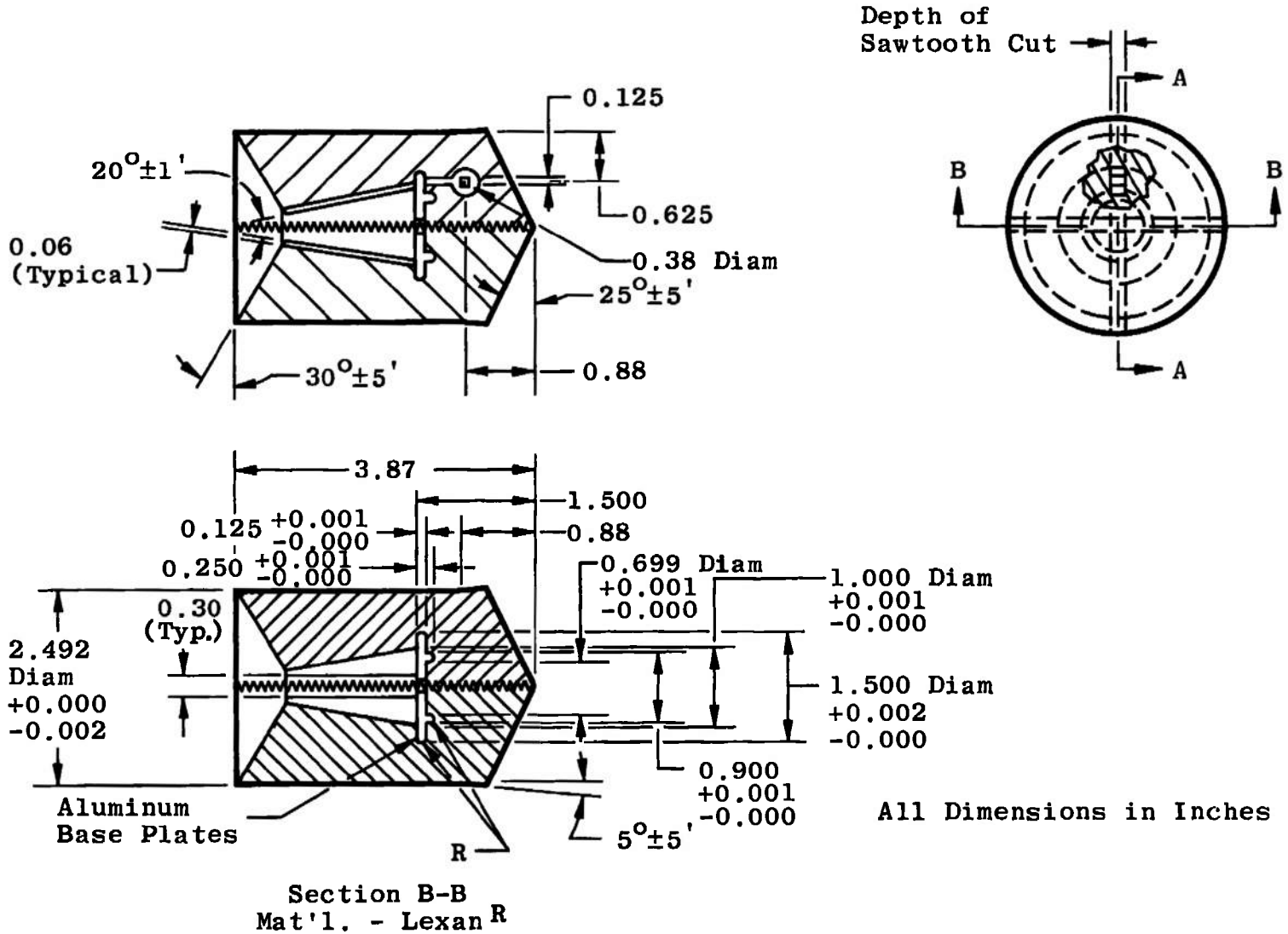

Fig. 20 Sabot for 10-deg Semiangle, 1.000-in. Base Diameter Cone Model

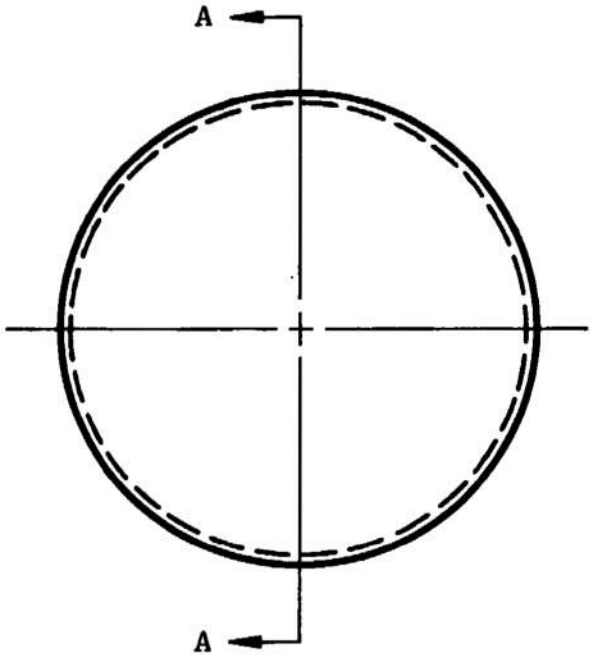

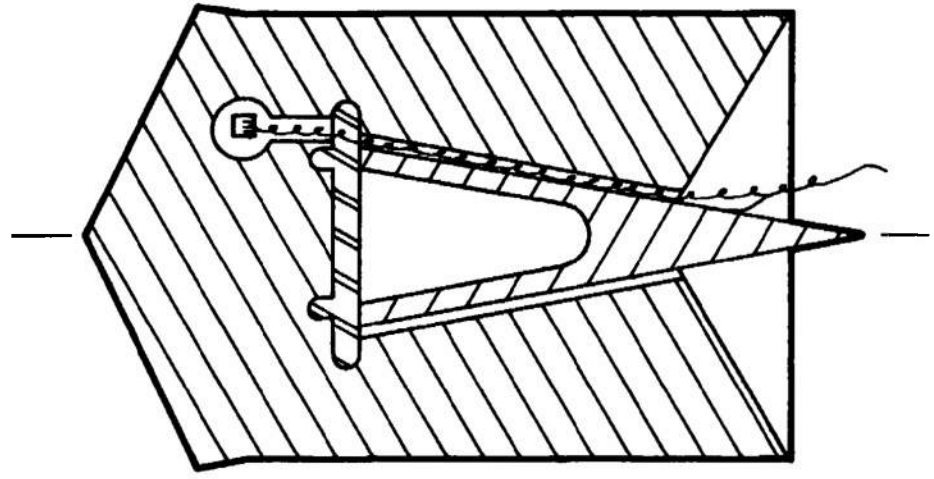

Section A-A

Fig. 21 Model-Sabot Package

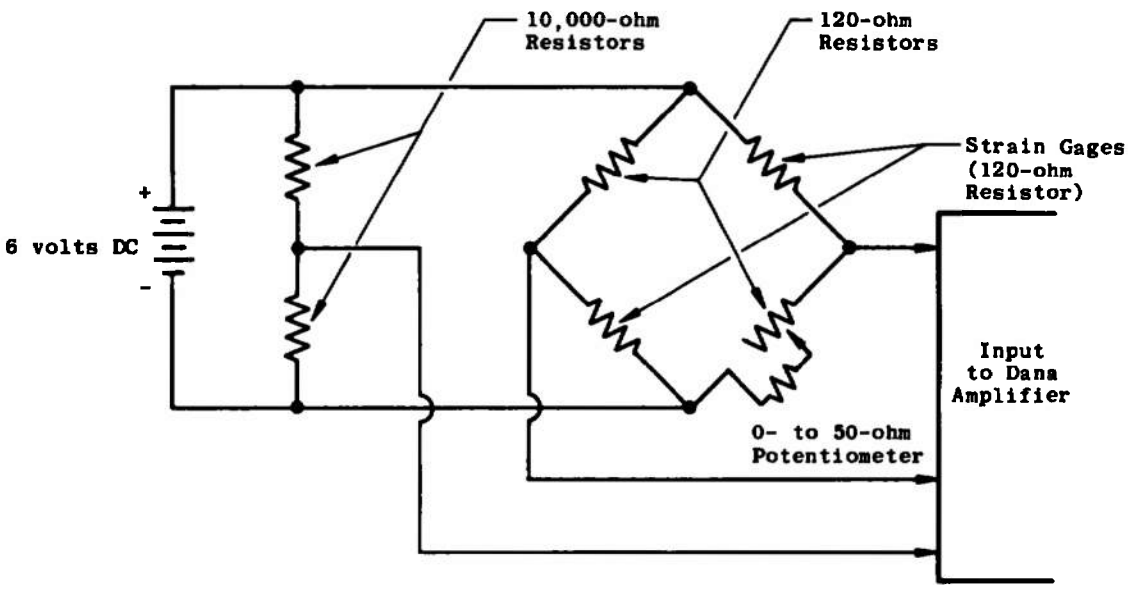

Fig. 22 Model Bridge Circuit

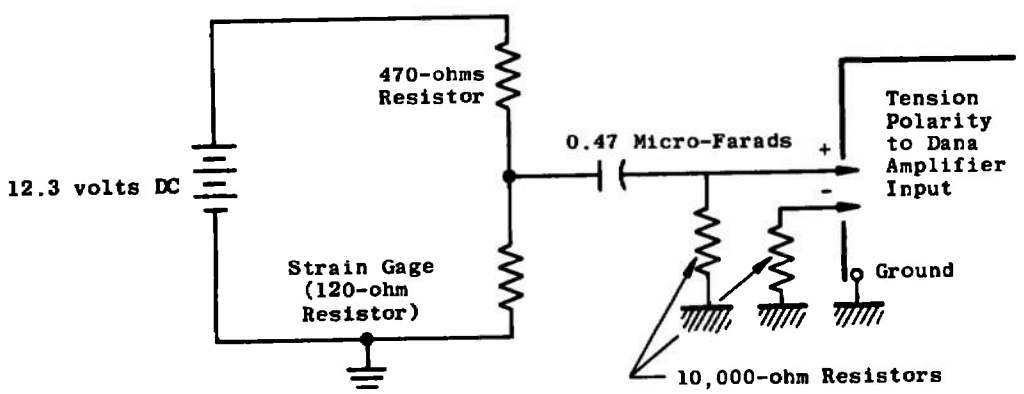

Fig. 23 Model-Sabot Potentiometer Circuit

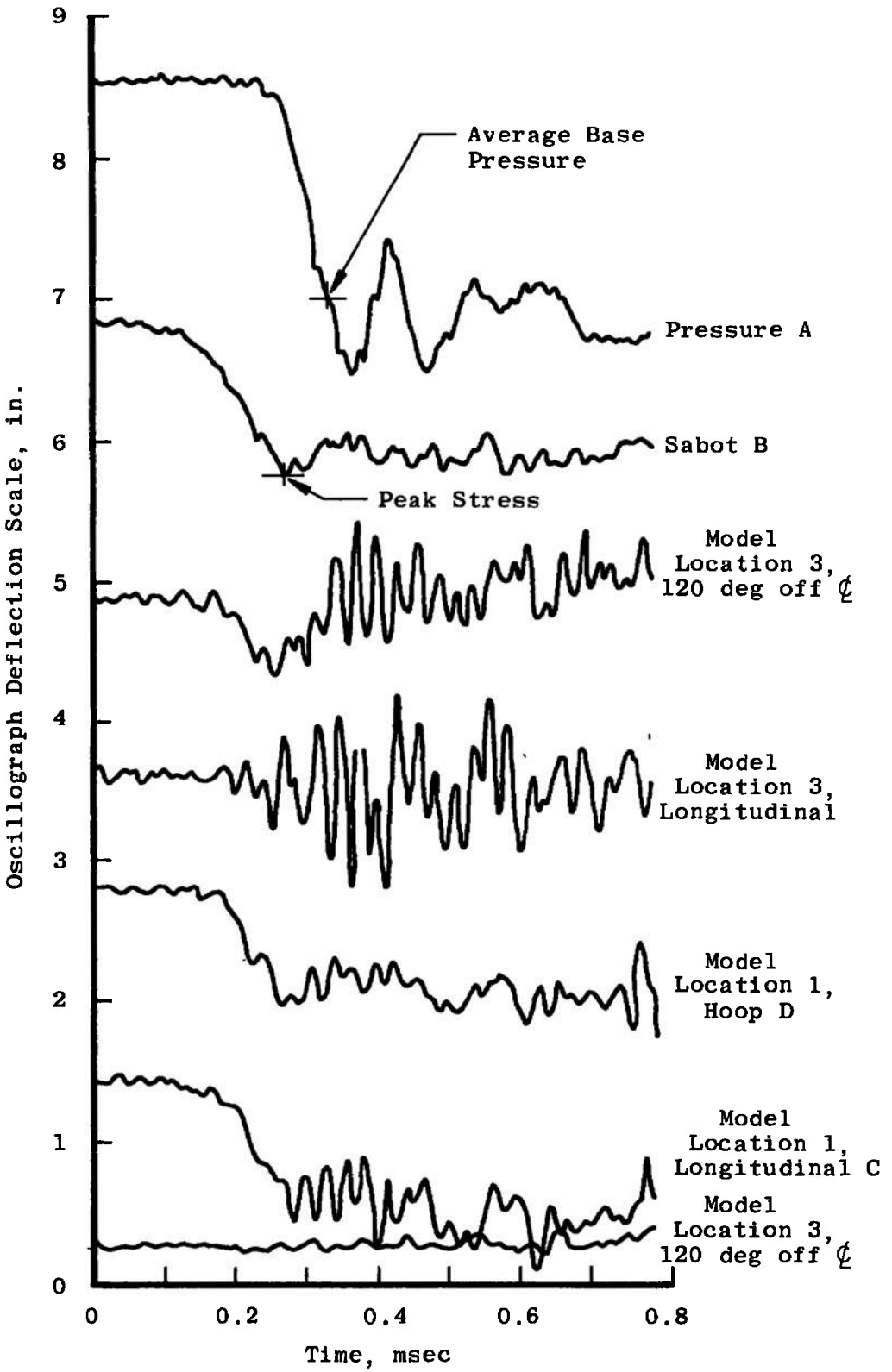

Fig. 24 Test 1 Data

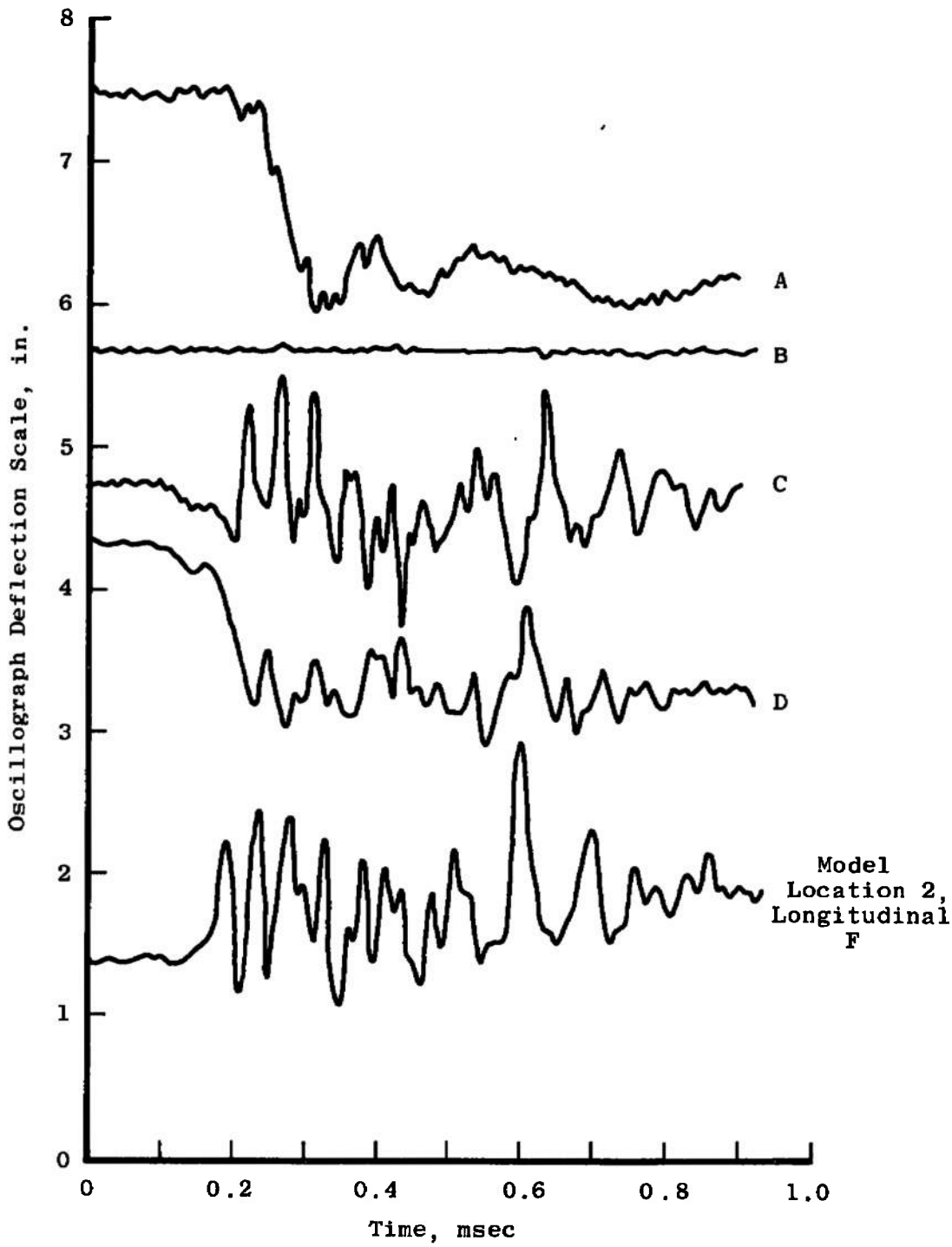

Fig. 25 Test 2 Data

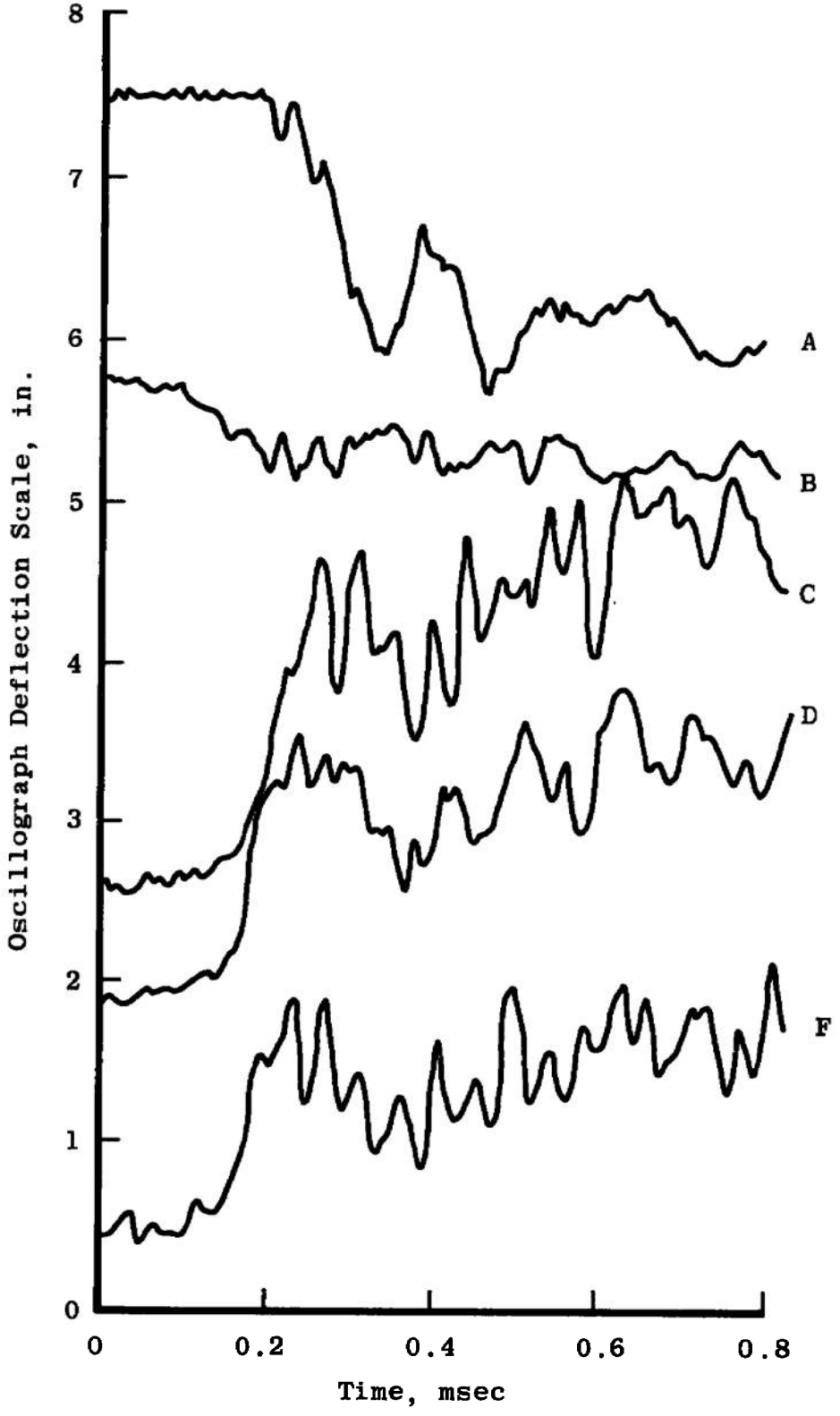

Fig. 26 Test 3 Data

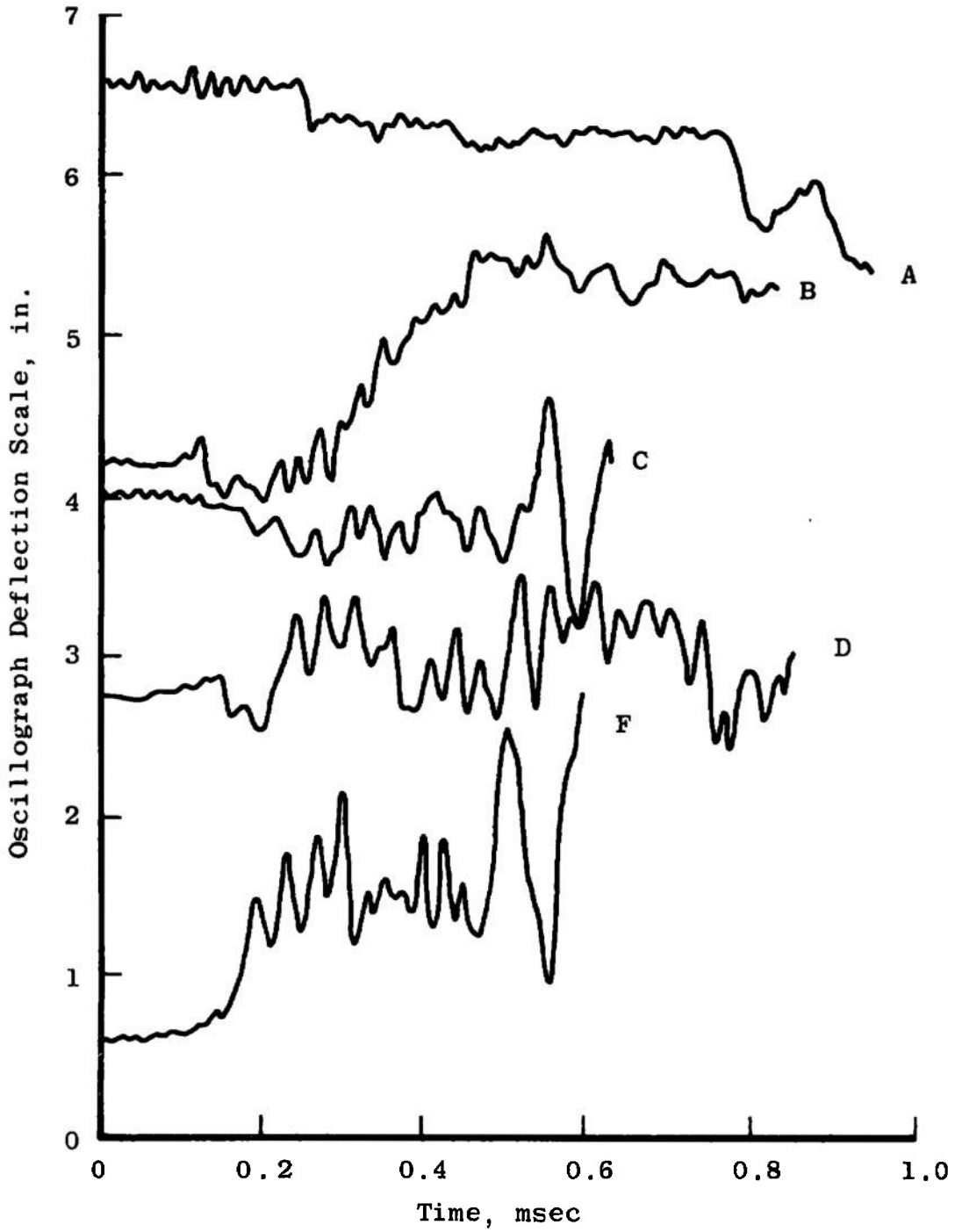

Fig. 27 Test 4 Data

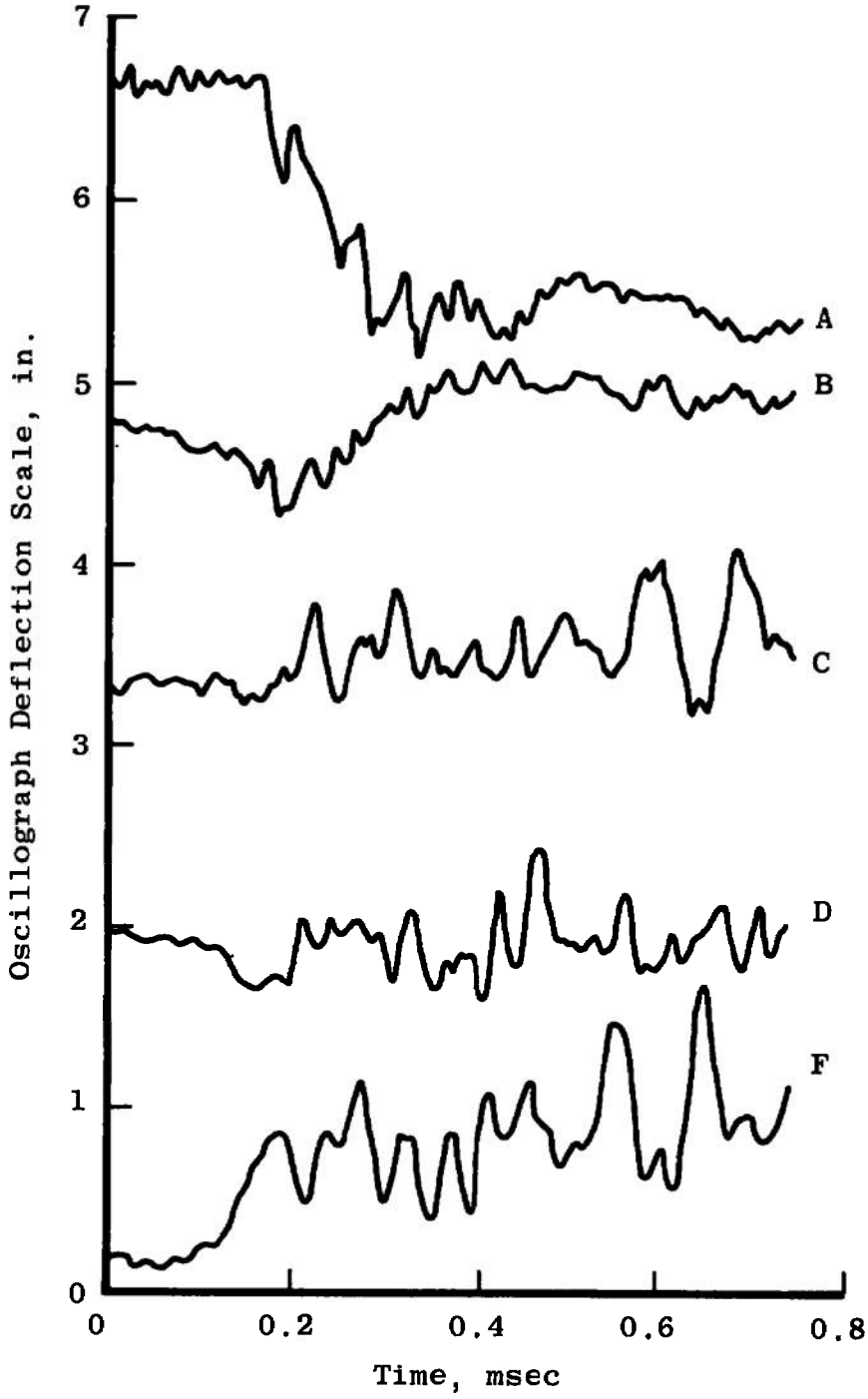

Fig. 28 Test 5 Data

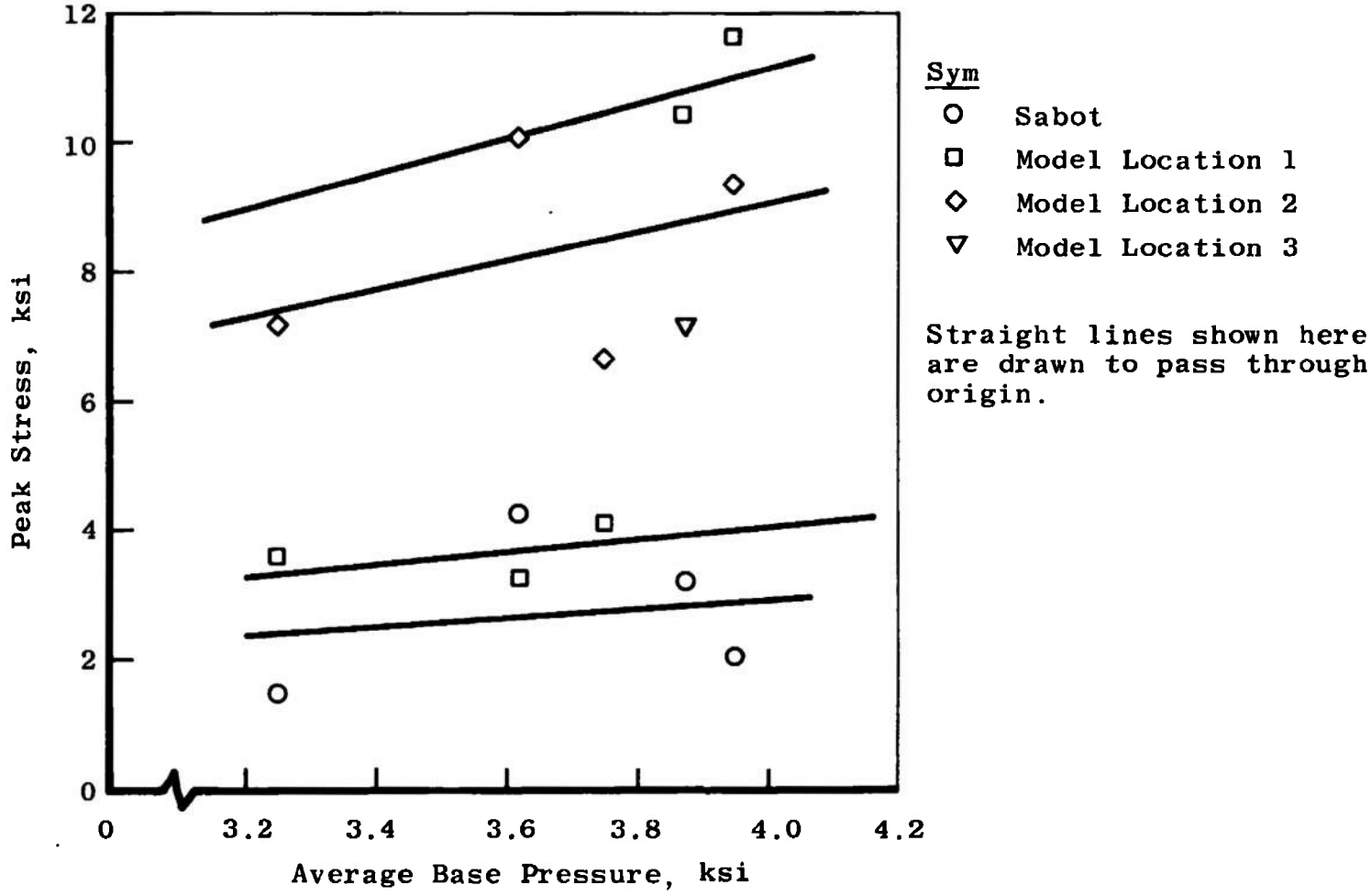

Fig. 29 Average Base Pressure versus Peak Stress

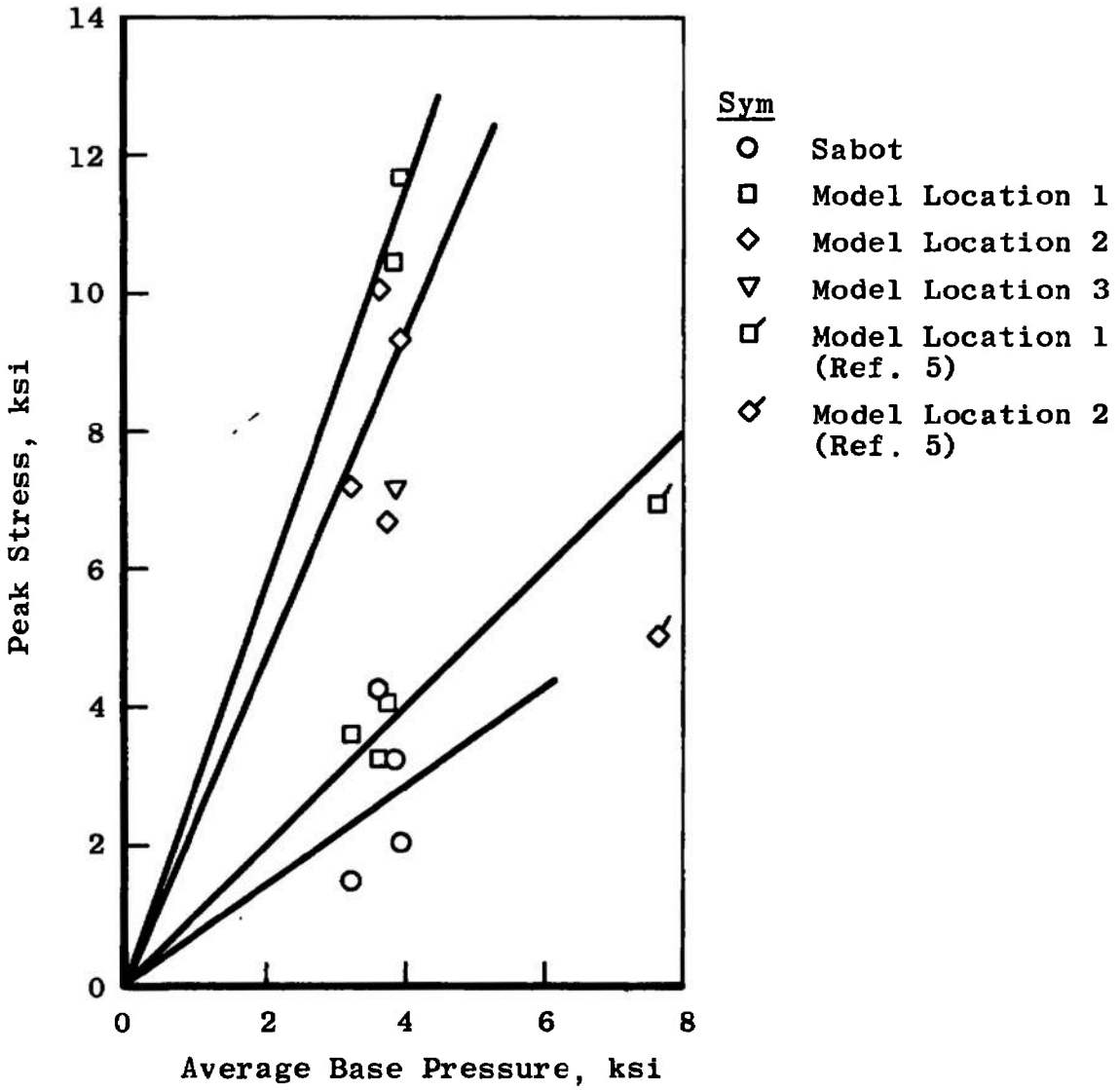

Fig. 30 Comparison with Ref. 5 of Average Base Pressure versus Peak Stress

TABLE I
MODEL–SABOT STRESSES

Test Number	Average Base Pressure (psi)	Longitudinal Peak Stress (psi)			
		Sabot	Model Location 1	Model Location 2	Model Location 3
1	3875	3220	10450	----	7160
2	3750	----	4075	6660	----
3	3950	2050	11660	9330	----
4	3621	4240	3230	10040	----
5	3250	1462	3590	7180	----

TABLE II
CALIBRATION DATA

Test No.	Location	Pressure (psi)	Voltage (volts)	Deflection (in.)
1	Pressure	5000		2
	Sabot		5	2
	Model 1 Longitudinal		5	1.8
	Model 1 Hoop		5	1.78
	Model 3 Longitudinal		5	2
	Model 3 120 deg off model centerline		5	1.9
	Model 3 120 deg off model centerline		5	2
2	Pressure	5000		2
	Sabot		5	2
	Model 1 Longitudinal		5.8	2.4
	Model 1 Hoop		5	2.1
	Model 2 Longitudinal		5.8	2.1
3	Pressure	5000		2
	Sabot		5	2
	Model 1 Longitudinal		5.8	2.4
	Model 1 Hoop		5	2.1
	Model 2 Longitudinal		5.8	2.1
4	Pressure	5000		2
	Sabot		5	2
	Model 1 Longitudinal		5.8	1.95
	Model 1 Hoop		5	2
	Model 2 Longitudinal		5.8	2
5	Pressure	5000		2
	Sabot		5	2
	Model 1 Longitudinal		5.8	1.95
	Model 1 Hoop		5	2
	Model 2 Longitudinal		5.8	2

APPENDIX III
CALIBRATION OF STRAIN GAGES

Figure 23 is a diagram of the potentiometer circuit used for strain gages on both the sabot and model.

The model strain gages were calibrated using a 5-mv signal and with 20.8 milliamp gage current, this indicated 1.28 milliamp/in. strain (Ref. 6); i.e., 3.91 μv is equivalent to 1 μ in./in. The strain gage signal was amplified by 1000 times to give a suitable input for the magnetic tape recorder.

The sabot strain gages were calibrated similarly but with a 50-mv signal corresponding to a strain of 12.6 millinch/in. for the same gage current (3.97 μv/μ in./in.), and the signal is then amplified 100 times before input to magentic tape recorder. This larger calibration signal is required because the sabot strain measured is an order of magnitude higher than those of the model.

The strain gage bridge circuit calibration followed Ref. 5. The bridge circuit was used only for model strain gages. The calibration constant is 5.84 μv per 1 μ in./in. strain.

APPENDIX IV
CALCULATION OF STRESS FROM STRAIN-GAGE DATA

As an example, the stress at location 1 (Fig. 19) for test number 1 will be computed. Table II shows the experimental voltage-oscillograph deflection calibration data for test number 1, and from Appendix III,

$$3.91\ \mu v = 1\ \mu \text{ in./in. strain}$$

From Table II,

$$1.8 \text{ in.} = 5 \text{ v (magnetic tape recorder)}$$
$$= 5 \text{ mv (signal)}$$

Thus,

$$\epsilon' = \frac{5 \times 10^3}{1.8 \times 3.91} = 711\ \frac{\mu \text{ in./in.}}{\text{in. (deflection)}}$$

Now the deflection from Fig. 24 for location 1 (longitudinal gage) will give the actual measured strain.

Deflection for peak stress is 1.05 in.

Thus,

$$\epsilon = \left(711 \frac{\mu \text{ in./in.}}{\text{in.}}\right)(1.05 \text{ in.}) = 746\ \frac{\mu \text{ in.}}{\text{in.}}$$

Now the stress can be found by means of the three-dimensional stress strain relationships.

$$\sigma_z = \frac{E}{1 - \mu - 2\mu^2}\left[\epsilon_z(1 - \mu) + \mu(\epsilon_r + \epsilon_\theta)\right]$$

Since the model and sabot are confined by the launch tube, both are axisymmetrical, and the loading is almost one-dimensional along the z axis. In other words, the plane-strain assumption for r and θ directions can be made; hence, ϵ_θ and ϵ_r are zero.

$$\therefore\ \sigma_z = \frac{E\,\epsilon_z(1 - \mu)}{1 - \mu - 2\mu^2}$$

For the model,

$$\mu = 0.3$$

$$E = 10.4\,(10)^6 \text{ psi}$$

and

$$\sigma_z = \frac{(10.4)\,(10)^6\,\epsilon_z\,(1 - 0.3)}{1 - 0.3 - 2\,(0.3)^2}$$

$$\sigma_z = \frac{(10.4)\,(10)^6\,\epsilon_z\,(0.7)}{0.52} = 14\,(10)^6\,\epsilon_z$$

$$\sigma_z = (14)\,(746) = 10,540 \text{ psi}$$

The same computational procedure is applied to the sabot as well as the other model locations.

UNCLASSIFIED

Security Classification

DOCUMENT CONTROL DATA - R & D

(Security classification of title, body of abstract and indexing annotation must be entered when the overall report is classified)

1 ORIGINATING ACTIVITY (Corporate author) Arnold Engineering Development Center Arnold Air Force Station, Tennessee 37389	2a. REPORT SECURITY CLASSIFICATION UNCLASSIFIED 2b. GROUP N/A

3 REPORT TITLE

HYPERVELOCITY LAUNCHER IMPROVEMENT TECHNIQUES

4 DESCRIPTIVE NOTES (Type of report and inclusive dates)

July 1970 to June 1972--Final Report

5 AUTHOR(S) (First name, middle initial, last name)

J. R. DeWitt and D. T Akers, ARO, Inc.

6 REPORT DATE December 1972	7a. TOTAL NO OF PAGES 50	7b. NO OF REFS 6
8a. CONTRACT OR GRANT NO b. PROJECT NO c. Program Element 65802F d.	9a. ORIGINATOR'S REPORT NUMBER(S) AEDC-TR-72-163 9b. OTHER REPORT NO(S) (Any other numbers that may be assigned this report) ARO-VKF TR-72-114	

10 DISTRIBUTION STATEMENT

Approved for public release; distribution unlimited.

11 SUPPLEMENTARY NOTES Available in DDC	12 SPONSORING MILITARY ACTIVITY Arnold Engineering Development Center, Arnold Air Force Station, Tennessee 37389.

13 ABSTRACT The purpose of this work was to reduce the damage to models caused by the launching accelerations in a hypervelocity launcher. A diaphragm test device was modified to better simulate conditions at diaphragm release in a hypervelocity launcher. Modification allowed hydrogen to be used as the test gas and a sabot to be placed in a short launch tube downstream of the diaphragm. Pressure transducers on both sides of the diaphragm were used to monitor the opening characteristics of various diaphragms. It was determined that diaphragms with tapered web thicknesses could be designed to produce pressure-time histories on the base of sabots that were less conducive to production of damaging transient stress waves in the sabots. The dynamic stress waves in a model and sabot and their interactions were measured experimentally in the diaphragm test device for a 10-deg semiangle cone model and sabot package typical of those launched in the AEDC 1000-ft Range G. Only the initial part of the motion in the launcher was duplicated using standard G-Range diaphragm, model, and sabot. The stresses were measured by strain gages cemented to portions of the model and sabot.

DD FORM 1 NOV 65 1473

UNCLASSIFIED

Security Classification

14. KEY WORDS	LINK A		LINK B		LINK C	
	ROLE	WT	ROLE	WT	ROLE	WT
test facilities						
hypervelocity launchers						
gun launchers						